Master's Thesis

Neutron XS Library Generation of ENDF/B-VIII.0 for MOC code STREAM and Monte Carlo code MCS

Kiho Kim

Department of Nuclear Engineering

Graduate School of UNIST

2019

Neutron XS Library Generation of ENDF/B-VIII.0 for MOC code STREAM and Monte Carlo code MCS

Kiho Kim

Department of Nuclear Engineering

Graduate School of UNIST

Neutron XS Library Generation of ENDF/B-VIII.0 for MOC code STREAM and Monte Carlo code MCS

A thesis/dissertation
submitted to the Graduate School of UNIST
in partial fulfillment of the
requirements for the degree of
Master of Science

Kiho Kim

Month/Day/Year of submission
Approved by

_____

Advisor
Deokjung Lee

Neutron XS Library Generation of ENDF/B-VIII.0 for MOC code STREAM and Monte Carlo code MCS

Kiho Kim

This certifies that the thesis/dissertation of Kiho Kim is approved.

07/05/2019 of submission

signature

_____

Advisor: Deokjung Lee

signature

_____

Fynan Douglas

signature

_____

Eisung Yoon

ABSTRACT

In this paper, the verification and validation of ENDF/B-VIII.0 XS data uses STREAM code and MCS code. ENDF/B-VIII.0 XS data compare with ENDF/B-VII.1 XS data. In the case of a library of unique nuclear data for STREAM, the neutron transport analysis code, ENDF files for each nuclide were produced in Group-wise XS using NJOY code system, and in the second step, STREAM XS Library was produced using STREAM library production system, NTOS. Using this multi-group nuclear data production system, STREAM XS library was produced for all nuclides based on ENDF/B-VII.1 nuclear data library and ENDF/B-VIII.0 nuclear data library. To assess the accuracy of the library, STREAM code and MCS code were simultaneously compared for each ENDF version.

For the validation, each of benchmarks are used, NCA benchmark, VERA benchmark and ICSBEP benchmark. NCA benchmark analysis, which is the critical experiments performed at the Toshiba Nuclear Critical Assembly (NCA) critical facility. Each benchmark was compared in STREAM and MCS, and NCA benchmark analysis include tungsten gray rods demonstrates the accuracy of STREAM code's pin power distribution. STREAM code nuclear source used the both of ENDF/B-VIII.0 and ENDF/B-VII.1, and their results compared with each of MCS code results.

When STREAM's results were compared for each version of ENDF, NCA benchmark found that the difference of the effective multiplication factor was within 100 pcm for the problem, confirming that ENDF/B-VIII.0 STREAM XS Library was properly produced. Also in case of VERA benchmark and ICSBEP benchmark, the difference of the effective multiplication factor was within 300 pcm for the problem with ENDF/B-VII.1 XS Library results and ENDF/B-VIII.0 XS Library results. The accuracy of STREAM results was verified by comparing them with the MCS results of the same problem for each result.

Key Words: **ENDF/B-VIII.0, STREAM, MCS, Critical experiments, Cross-section Library**

CONTENTS

I. INTRODUCTION

Numerical analysis of the reactor's behavior is essential for the design and safe and economical operation of the actual reactor. Numerical analysis should incorporate an effective methodology to predict reactor behavior as accurately and rapidly as possible. Neutron behavior analysis is the most basic part of the reactor analysis methodology related to these, and the neutron behavior analysis is based on the nuclear data library. This is why the nuclear data library have to accurate. It is very important to produce an accurate nuclear data library because, no matter how effective the method is, the wrong library cannot properly predict the state of the reactor.

Recently, the Cross Section Evaluation Working Group (CSEWG) released a new revision of ENDF/B evaluated nuclear data library, ENDF/B-VIII.0. Therefore, for the evaluation of new nuclear data, the existing library of ENDF/B-VII.1 nuclear data needs to be compared and contrasted with ENDF/B-VIII.0 that was recently released.

Some of the nuclides that make up the reactor exist in areas where the XS changes rapidly with changes in energy, and these rapid changes have a significant effect on the neutron flux. Therefore, it is very important to identify the exact difference between the newly released ENDF/B-VIII.0 nuclear data library and the existing ENDF/B-VII.1 nuclear data library.

In this study, the multi-group nuclear data integrated production system was established to supply the highly accurate nuclear data to STREAM calculation, and the results were verified by Monte Carlo Code MCS for each problem results.

In order to validate the results of each XS difference, the neutron transport analysis code STREAM developed by UNIST and the Monte Carlo code MCS developed by UNIST were used. For a brief introduction about each codes, MOC code, STREAM (Steady state and Transient REactor Analysis code with Method of characteristics) has been developed at Ulsan National Institute of Science and Technology (UNIST). STREAM code has been developed to perform a light water reactor core analysis with direct transport one-step method and transport/diffusion two-step method. Numerous advanced features have been developed and

implemented in the STREAM code for higher accuracy and performance. Monte Carlo Whole core analysis code, MCS also has been developed at Ulsan National Institute of Science and Technology (UNIST). MCS was developed for Large Scale Reactor Analysis through accelerated Monte Carlo simulation. It is equipped with multi-physics function that combines CTF and FRAPCON, which enables the calculation of deletion to be performed and demonstrated accuracy through a number of all core simulations, including BEAVERS and VERA benchmarks.

The composition of this paper is as follows: Chapter 2 introduces the library of ENDF/B-VIII.0 nuclear data and discusses its differences from ENDF/B-VII.1. It first introduces several nuclides as criteria for compiling ENDF/B-VIII.0 and also addresses nuclides that had large differences in cross-sectional area in the core analysis of steady state in other areas. Chapter 3 describes the code used in this study, and Chapter 4 describes the integrated production system of STREAM-specific nuclear data within the STREAM code and how to produce the XS Library. Chapters 5 and 6 describe the effects of ENDF/B-VIII.0 evaluated nuclear data and ENDF/B-VII.1 evaluated nuclear data on each nuclear species, and how the changes affect them. Chapter 7 describes the benchmarks used for verification and Chapter 8, Chapter 9, and Chapter 10 describes the results of various benchmarks. Chapter 10 presents the conclusions of this study and discusses the tasks to be carried out in the future.

II. DESCRIPTION OF ENDF/B-VIII.0

ENDF/B-VIII.0 evaluated nuclear data library fully incorporates the new IAEA standards, includes improved thermal neutron scattering data and uses new evaluated data from the CIELO project for neutron reactions on 1H, 16O, 56Fe, 235U, 238U and 239Pu described in companion papers in the present issue of Nuclear Data Sheets. The Collaborative International Evaluation Library Organization coordinated by the Nuclear Energy Agency (NEA) Working Party has stimulated advances to the neutron cross-section evaluations of nuclides. The primary motivation for the CIELO project was the desire to more-rapidly expedite improvements in these important cross sections. Improving the evaluated data for such nuclides is a major undertaking, desired by nuclear science and technology communities around the world. The evaluations benefit from recent experimental data obtained in the U.S. and Europe, and improvements in theory and simulation. Notable advances include updated evaluated data for light nuclei, structural materials, actinides, fission energy release, prompt fission neutron and γ-ray spectra, thermal neutron scattering data, and charged-particle reactions. Integral validation testing is shown for a wide range of criticality, reaction rate, and neutron transmission benchmarks. In general, integral validation performance of the library is improved relative to the previous ENDF/B-VII.1 library.

Below is the number of materials present in each sublibrary in each release.

Table 1. Overview of the ENDF/B Library releases and the sublibraries

Sublibrary name	VIII.0	VII.1	VII.0	VI.8
Neutron	557	423	393	328
Thermal scattering	34	21	20	15
Proton	49	48	48	35
Deuteron	5	5	5	2
Triton	5	3	3	1
^{3}He	3	2	2	1
^{4}He	1	-	-	-
Photonuclear	163	163	163	-
Photo-atomic	100	100	100	100
Atomic relaxation	100	100	100	100
Electro-atomic	100	100	100	100
Radioactive decay	3821	3817	3838	979
Spont. fis. yields	9	9	9	9
Neutron fis. yields	31	31	31	31
Standards	10	8	8	8

The previous ENDF/B-VII.1 library was built in a variety of ways than the initial ENDF/B-VII.0 library. However, for all of these upgrades, previous ENDF/B-VII.1 preserved most of the ENDF/B-VII.0 library functions, the most notable major measures were not changed, and VII.1 typically required to preserve and improve the required good critical performance tests seen in ENDF/B-VII. However, many upgrades for important nuclides such as Actinide and several nuclides in the core required efforts to develop current ENDF/B-VIII.0.

The new ENDF/B-VIII.0 library, in contrast to ENDF/B-VII.1, has major changes in neutron response to other nuclides and major actions affecting nuclear materiality simulations. Important isotopes1H, 16O, 56Fe, 235,238U and 239Pu have been the focus of international CIELO collaboration, and the progress of the results have been incorporated into ENDF/B-VIII.0. Other notable developments in ENDF/B-VIII.0 that will not be explained in this paper include updating thermo-neutron scattering data that forms neutron responses to micro-organisms, structural materials, transversals of hard core, dosimetry, fission energy emissions, decay data, charge particle reactions, and low-energy molecules.

Below is the biggest changes with ENDF/B-VIII.0 and ENDF/B-VII.1.

- **CIELO evaluation** : New $^{1}\mathbf{H}$, $^{16}\mathbf{O}$, $^{56}\mathbf{Fe}$, $^{235}\mathbf{U}$, $^{238}\mathbf{U}$, $^{239}\mathbf{Pu}$ neutron reactions changed, including prompt fission neutron spectra and prompt fission gamma spectra.

Added the integral of the $^{235}\mathbf{U}$(n,f) cross section from 7.8–11 eV as a standard

Added high energy fission reference cross sections $^{235}\mathbf{U}$ (n,f), $^{238}\mathbf{U}$(n,f) from 200 MeV up to 1 GeV

- **Light elements** : New *n*, $^{2}\mathbf{H}$, $^{3}\mathbf{He}$, $^{6}\mathbf{Li}$, $^{9}\mathbf{Be}$, $^{10}\mathbf{B}$, $^{12,13}\mathbf{C}$ (tuned to match $^{nat}\mathbf{C}$ standards), $^{18}\mathbf{O}$, and $^{35,37}\mathbf{Cl}$;
- **Structural materials**: New $^{40}\mathbf{Ca}$, constituents of steel ($^{54,56,57,58}\mathbf{Fe}$, $^{58-62,64}\mathbf{Ni}$), $^{59}\mathbf{Co}$, $^{63,65}\mathbf{Cu}$, $^{174-182}\mathbf{Hf}$, $^{182-186}\mathbf{W}$ (resonance parameter evaluation in 1e-5 eV to 10 keV) and revised $^{105}\mathbf{Rh}$, $^{132}\mathbf{Te}$
- **Rare earths**: Adopted **Dy** and **Yb** from JENDL-4.0
- **Noble gases**: Revised $^{40}\mathbf{Ar}$, $^{78}\mathbf{Kr}$, $^{124}\mathbf{Xe}$; $^{20-22}\mathbf{Ne}$ from TENDL-2015
- **Minor actinides**: New $^{236m}\mathbf{Np}$, $^{240}\mathbf{Pu}$, new nubars and revised $^{241,243}\mathbf{Am}$

- **Misc. materials**: New $^{73-75}$**As** and ^{197}**Au**; $^{190-198}$**Pt** adopted from TENDL-2015
- **Unstable isotopes**: Added all isotopes with $T_{1/2} \geq 1$ year and all the intermediate nuclei needed to produce these isotopes through neutron-induced reactions using a combination of TENDL-2015 evaluations and EMPIRE calculations
- **Primary gammas**: Added to ^{6,7}**Li**, ^{11}**B**, ^{19}**F**, ^{23}**Na**, ^{27}**Al**, ^{28}**Si** and ^{35,37}**Cl** to support nondestructive assay applications
- Additionally, at the Thermal Scattering law sublibrary,

Fuels: New UO2 and UN

Moderators: New heavy and light water, graphite (reactor grade and crystalline), polyethylene, lucite, and yttrium hydride

Reflectors: Revised Be and BeO

Natural materials: New ice and SiO2

Cladding: New SiC

In this study, the five nuclides of the CIELO project, as well as the light elements and structural materials contained in the benchmark, are to be verified.

III. CODE DESCRIPTION

3.1. STREAM

A neutron transport analysis MOC code, STREAM (Steady state and Transient REactor Analysis code with Method of Characteristics), was developed at UNIST. STREAM adopted several newly developed resonance self-shielding methods.

MOC Lattice physics codes are used to generate cross section data for nodal codes,where the nodal codes are used to model the coupled neutronics and thermal-hydraulics behavior of the entire reactor core during steady state and transient operation. Once the flux distribution is known, the cross sections can be condensed and homogenized into the structure needed by the nodal code. The nodal code then pieces the various lattices together to construct the various fuel assemblies in the reactor core.

STREAM has been developed to perform a whole LWR core calculation with the direct transport analysis method and the two-step method. Numerous advanced features, especially resonance treatment methods, have been developed and implemented in the STREAM code for higher accuracy and performance. STREAM with the advanced methods has order of ~100 pcm accuracy in LWR analyses. STREAM has capabilities to analyze the whole LWR core through the two-step (with PARCS or RAST-K 2.0) method and direct transport method (2-D).

It has several features: **Multi-group Cross-Section Generation** (Pin-based pointwise energy slowing-down method, Equivalence theory for structure material, Resonance upscattering correction, Enhanced neutron current method, Inflow transport correction), **Transport Solver** (Method of Characteristics, T-Y optimum quadrature sets, Assembly modular ray tracing method, Direct neutron path linking method, P0~P5 scattering source treatment, Coarse mesh finite difference acceleration), **Depletion** (Matrix exponential method, Chebyshev rational approximation method, Chain with ~1400 isotopes, Predictor/corrector), and **Few-group Constants Generation** (Discontinuity factor, Two-group cross-sections, Critical spectrum with fundamental mode calculation).

In STREAM, Pin-based Slowing-down Method (PSM) is newly developed method for solving slowing down problem and it is more accurate method than other method.

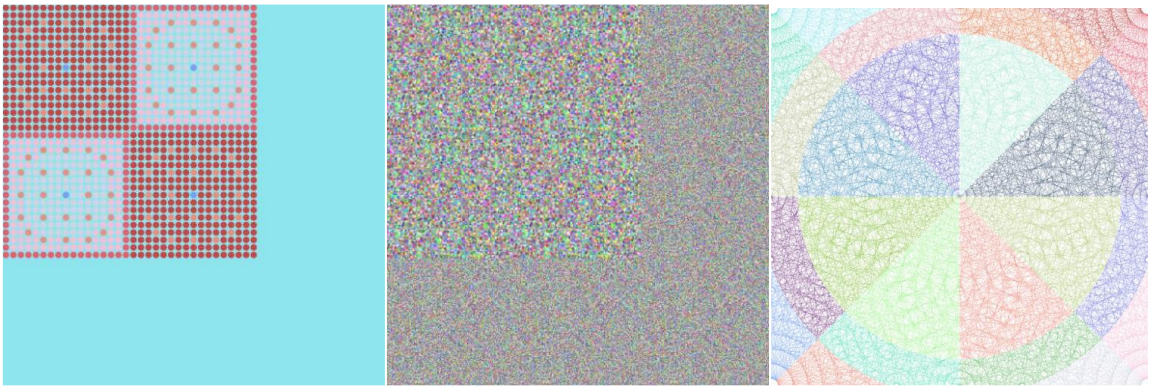

Figure 1. (1) MOC code 2-dimensinal quarter core design, (2) Ray tracing design for quarter core (3) Ray tracing for one pin.

3.2. MCS

A whole core analysis Monte Carlo code, MCS was developed at UNIST. MCS code has developed for Large Scale Reactor Analysis with accelerated Monte Carlo simulation.

It has several features: Neutron and Photon Transport, General 3-D geometry (CSG), Surface tracking & woodcock delta tracking, Resonance upscattering (DBRC, FESK), Probability table method, T/H coupling with CTF and FRAPCON, MOC and MC Hybrid solver acceleration, CMFD and Depletion (CRAM solver, Parallel Burnup, Quadratic Depletion, Equilibrium Xenon)

Due to these characteristics, the MCS code has various functions. MCS is capable of power reactor simulation with full feedbacks such as depletion, OTF cross-section, equilibrium xenon, critical boron search. MCS can be used for various purposes such as whole core simulation (Thermal reactor, Fast reactor, research reactor, etc.) and CASK analysis (neutron and photon simulation). Also, MCS is very efficient for large scale simulation: Tally overhead is very small for whole core simulation. The parallel efficiency is ~100% (up to 1,500 processors), Memory requirement is less than other MC codes.

For verification of the MCS code, Monte Carlo codes such as McCARD, OpenMC, Serpent, MCNP, KENO is used, and the accuracy of MCS whole core analysis is interpretated..

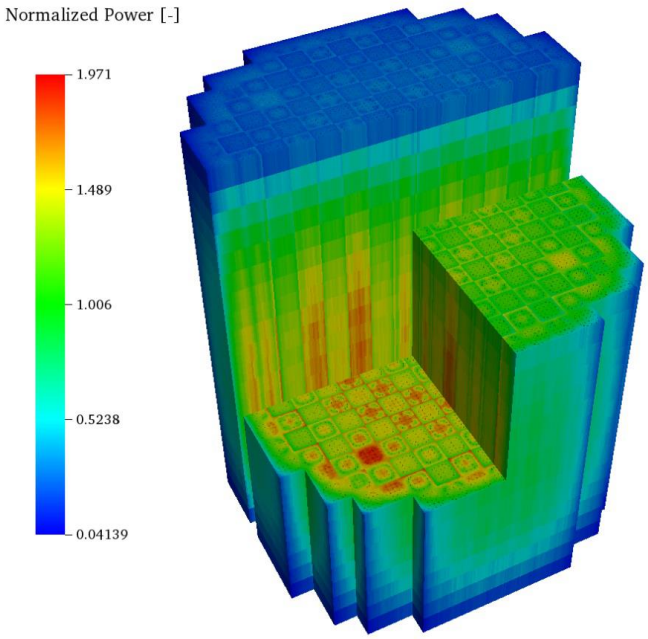

Figure 2. 3D whole core design figure for Monte Carlo code

IV. STREAM ENDF/B-VIII.0 LIBRARY GENERATION PROCESSING WITH NJOY2016

The production and analysis of nuclear data was carried out using the high-performance neutron core analysis code STREAM (Study state and Transient REactor Analysis Code with Method of Characters). The nuclear cross-sectional production system for core calculation was developed, and a high-precision multi-group nuclear cross-section library has produced.

In STREAM, multi-group nuclear cross-sectional data is produced using NJOY, a nuclear data production code, and the data is reprocessed through its own nuclear cross-section library production system to produce a library. STREAM codes derive the solution of the neutron transport equation using a library of nuclear cross-sectional areas produced so that high accuracy core calculation through resonance processing, neutron dynamic factor and reactivity ulcer calculation are carried out. Figure 1-1 shows the STREAM code computing system.

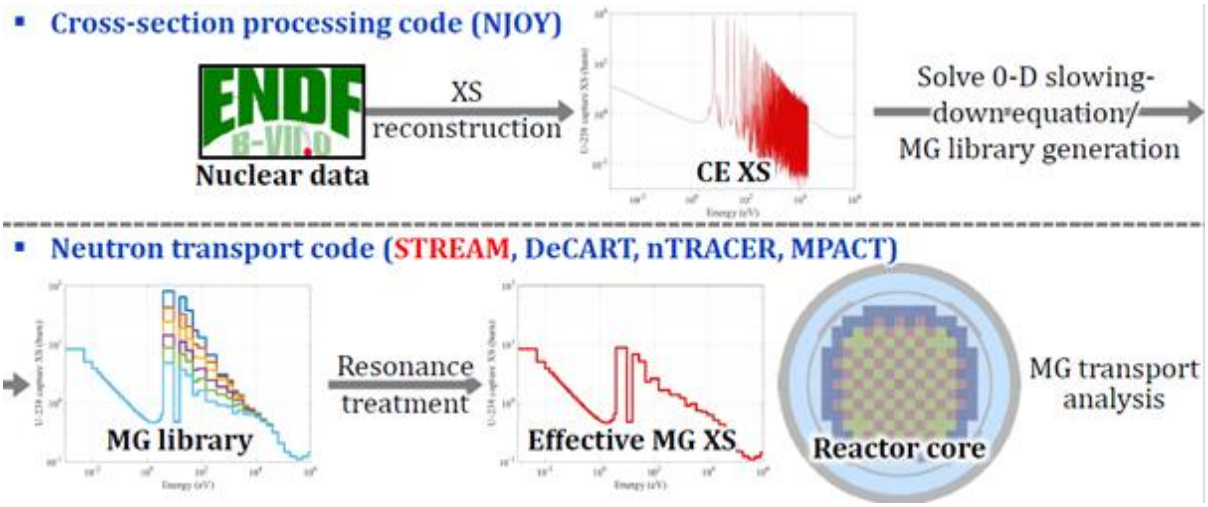

Figure 3. 1-Step STREAM Neutron Transport Analysis Computing System

NJOY Nuclear Data Processing System is a comprehensive computer code package for producing pointwise and multigroup cross sections and related quantities from evaluated nuclear data in the ENDF-4 through ENDF-6 formats. NJOY works with evaluated nuclear data for incident neutrons, photons, and charged particles, producing libraries for a wide variety of particle transport and reactor analysis codes.

NJOY is a modular program, with a variety of subprograms each performing a unique task in a multistep sequence. The ENDF files processed here used NJOY modules such as MODER, RECONR, BROADR, UNRESR, THERMR, GROUPR. Below is the descriptions of each modules.

MODER converts ENDF "tapes" back and forth between ASCII format and the special NJOY blocked-binary format.
RECONR reconstructs pointwise (energy-dependent) cross-sections from ENDF resonance parameters and interpolation schemes.
BROADR Doppler broadens and thins pointwise cross sections.
UNRESR produce effective self-shielded cross sections for resonance reactions in the unresolved energy range.
THERMR module generates pointwise neutron scattering cross sections in the thermal energy range and adds them to an existing PENDF file.
GROUPR generates self-shielded multi-group cross sections, group-to-group scattering matrices, photon production matrices, and charged-particle multi-group cross sections from pointwise input.

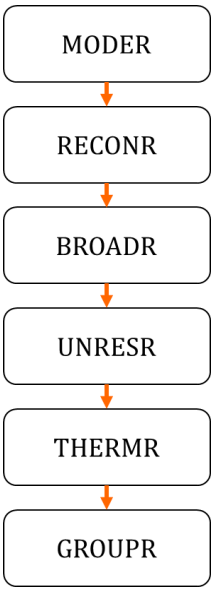

Figure 4. Flow diagram of NJOY2016 processing for STREAM 72G multi-group library generation

Next step is using NTOS code. NTOS is XS library generation code for STREAM. The NTOS reproduces reprocessed nuclear cross-sectional data from NJOY into a library format for STREAM. In order to reduce the need for STREAM internal calculations, the NTOS itself collects and processes nuclear cross-nucleus from NJOY nuclear data to produce a library.

The nuclear cross-sectional processing inside the NTOS is performed by temperature and by nuclide from the output file from NJOY, and the XSs are:

(1) From the P0 scatting matrix to the P3 scatting matrix, calculate the total ratio of each P0~P3 scattering matrixes of discrete inelastic scattering XS, (n,2n) scattering XS, (n,3n) scattering XS, and multiply and save it with the original XS value of each energy group

(2) Add inelastic scattering XS, (n,2n) XS * 2, (n,3n) XS * 3 to the elastic scattering XS produced.

(3) Replace the calculated free thermal scattering XS in the resonance area with elastic scattering XS. This omits the nuclear cross-section data of the parts not required and calculates the required nuclear cross-section from the core transport analysis in advance.

Through this processes, a STREAM 72G multi-group nuclear data library of ENDF/B-VIII.0 has produced. In addition, because ENDF/B-VIII.0 has calculated only as NJOY2016, ENDF7.1 has also calculated as NJOY2016 to prevent errors from NJOY versions.

V. ENDF/B-VIII.0 AND ENDF/B-VII.1 URANIUM XS DATA COMPARISON

Using the STREAM multi-group XS library production system, a STREAM XS library has produced for critical nuclides based on the ENDF-B/VIII.0 nuclear data library. Therefore, in this chapter, we will compare XS produced using the 72G STREAM XS library and compare reactivity through a simple pin problem test.

When compared with the 4.9w/o fuel pin test results used in the NCA benchmark, the difference in total reactivity between ENDF/B-VIII.0 and ENDF/B-VII.1 is as shown in Figure 5. The difference in reactivity in the thermal region can be seen to have many effects on XS changes in Uranium 235. The difference in reactivity in each group is not a small effect, so in this chapter we would like to see what changes and their impact on the XS of uranium under the versions of ENDF.

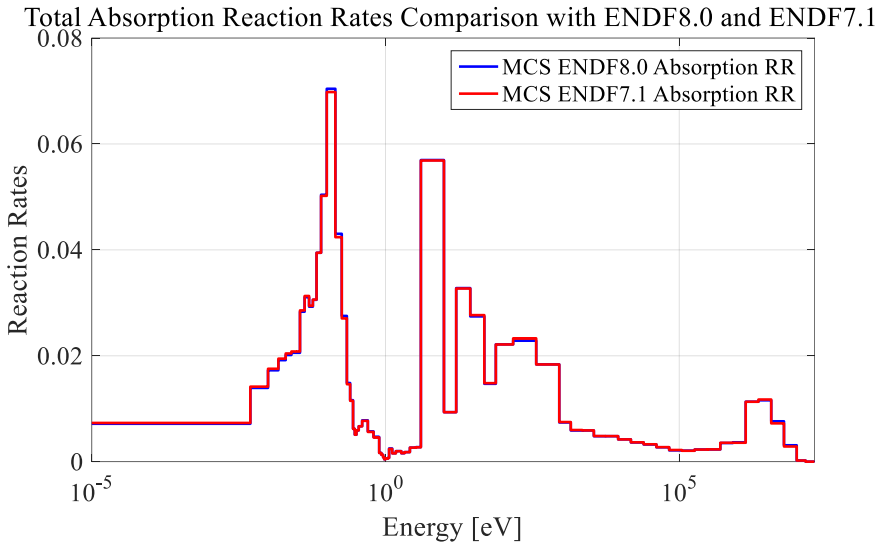

Figure 5. Total Absorption Reaction Rates Comparison of 4.9w/o fuel pin with ENDF/B-VIII.0 and ENDF/B-VII.1

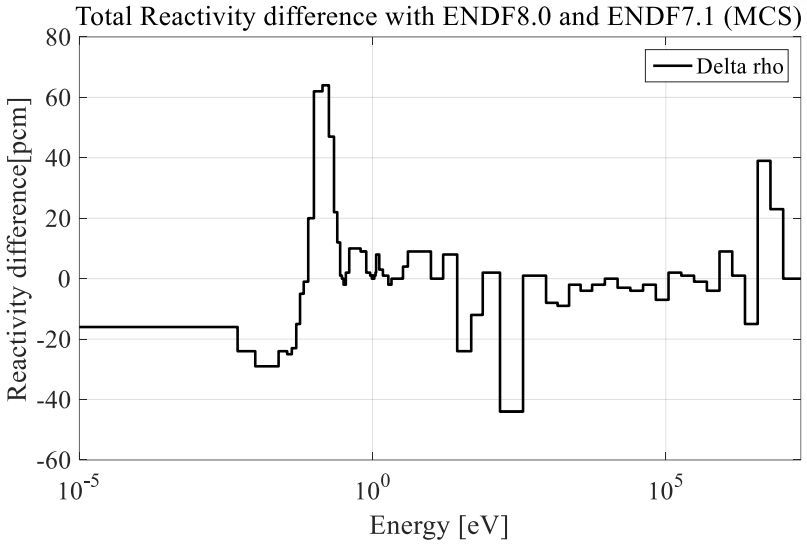

Figure 6. Total Reactivity difference of 4.9w/o fuel pin with ENDF/B-VIII.0 and ENDF/B-VII.1

5.1. U-238 Total XS

Uranium 238 is the most important nuclide responsible for the Background of nuclear fuel, and simulation results can respond sensitively to changes in Uranium 238 XS in ENDF version. Under 3.3eV energy range, XS difference is 0.5% lower averagely, and at the resonance energy range over 4.0eV, the U-238 XS difference between ENDF/B-VIII.0 and ENDF/B-VII.1 is not organized. The resonance region of U-238 is approximately under 0.022MeV and except the XS of 906.8eV-142.5eV, most of U-238 total XS of ENDF/B-VIII.0 at resonance region is higher than U-238 total XS of ENDF/B-VII.1. The noticeable point of U-238 of ENDF/B-VIII.0 as compare with ENDF/B-VII.1, the difference of Fission XS at 906.8eV-5530eV is almost 700% for maximum. Averagely under resonance and thermal region, the difference of thermal scattering XS is about 0.642%.

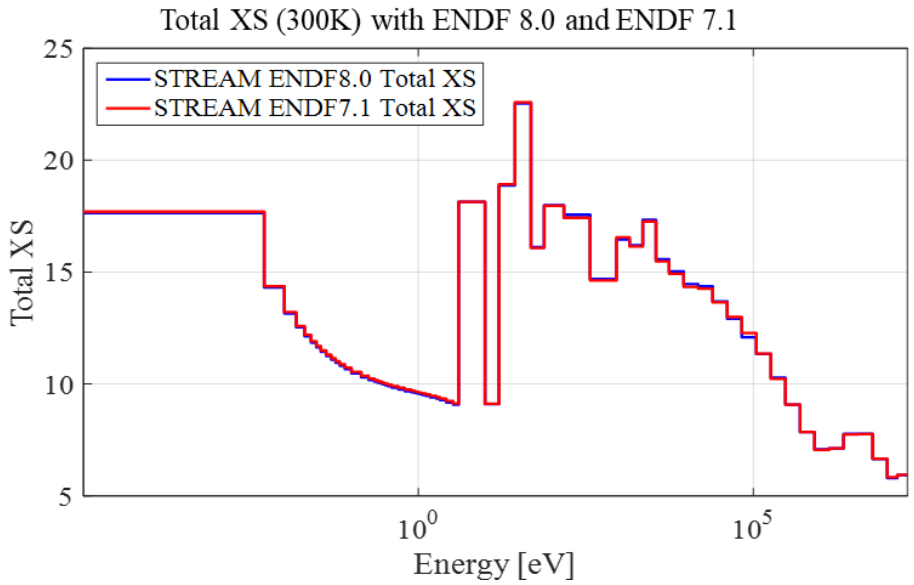

Figure 7. U-238 Total XS with ENDF/B-VIII.0 and ENDF/B-VII.1 at 300K

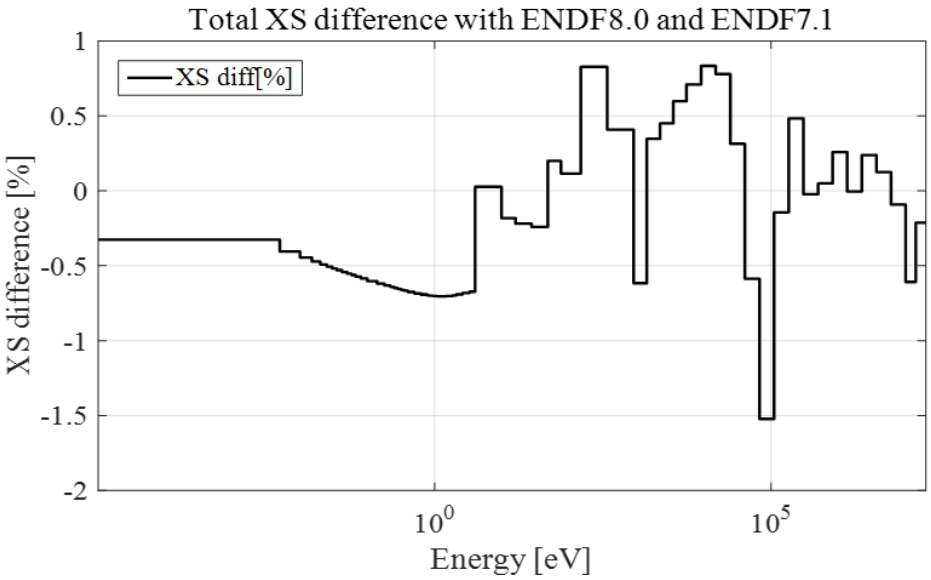

Figure 8. U-238 Total XS difference with ENDF/B-VIII.0 and ENDF/B-VII.1 at 300K

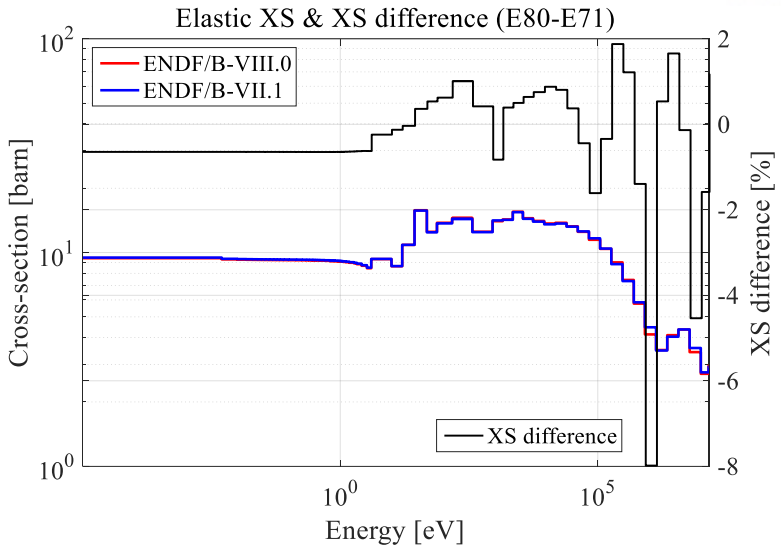

Figure 9. U-238 Elastic XS and XS difference with ENDF/B-VIII.0 and ENDF/B-VII.1 at 300K

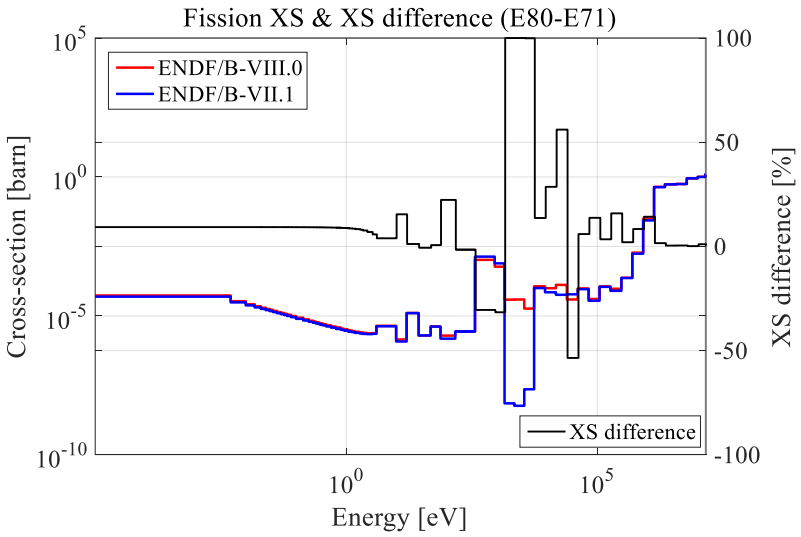

Figure 10. U-238 Fission XS and XS difference with ENDF/B-VIII.0 and ENDF/B-VII.1 at 300K

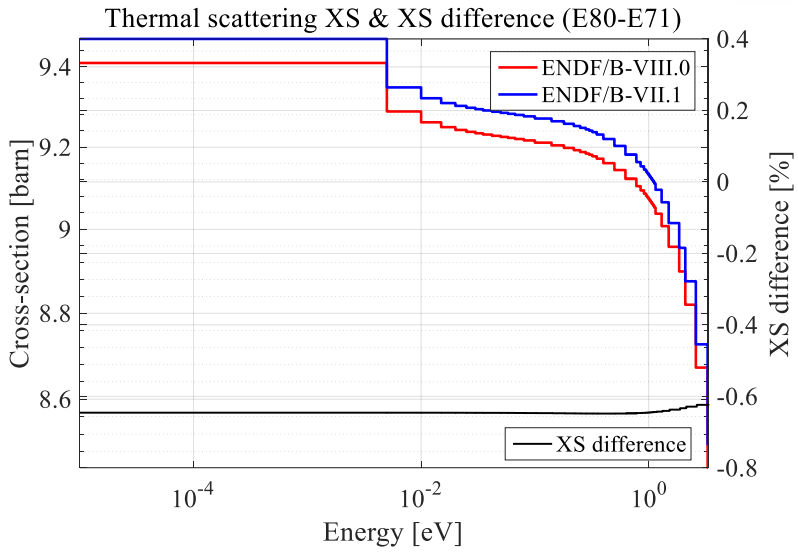

Figure 11. U-238 Thermal scattering XS and XS difference with ENDF/B-VIII.0 and ENDF/B-VII.1 at 300K

5.2. U-238 Absorption Reaction Rates Comparison with ENDF/B-VIII.0 and ENDF/B-VII.1

5.2.1. STREAM – U-238 Absorption RR & Reactivity difference

As compare with U-238 absorption reaction rates and reactivity difference between ENDF/B-VIII.0 and ENDF/B-VII.1, 4.9% w/o NCA pin is used. Reactivity difference of each group between ENDF/B-VIII.0 and ENDF/B-VII.1 is within allowable range such as -61 pcm and total reactivity difference is about -420 pcm in STREAM.

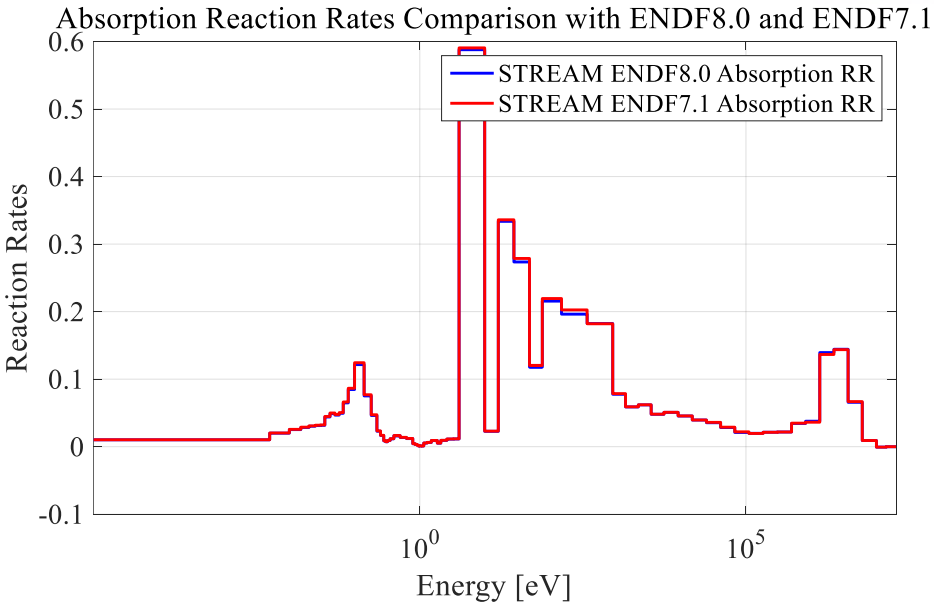

Figure 12. U-238 Absorption Reaction Rates Comparison of 4.9w/o fuel pin with ENDF/B-VIII.0 and ENDF/B-VII.1 in STREAM

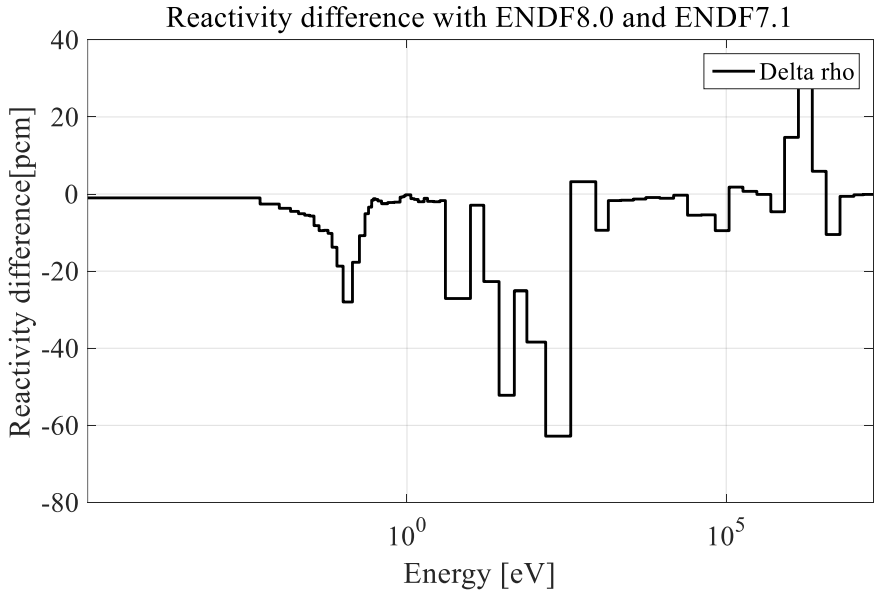

Figure 13. U-238 Reactivity difference of 4.9w/o fuel pin with ENDF/B-VIII.0 and ENDF/B-VII.1 in STREAM

5.2.2. MCS – U-238 Absorption RR & Reactivity difference

MCS is using ACE XS files generated from NJOY. Therefore, the Reactivity difference of MCS can be different with the reactivity difference of STREAM. The Figure 12 & 13 is

tallied value with STREAM 72 group energy boundary. Reactivity difference of each group between ENDF/B-VIII.0 and ENDF/B-VII.1 is within allowable range such as 100 pcm and total reactivity difference is about 296 pcm in MCS.

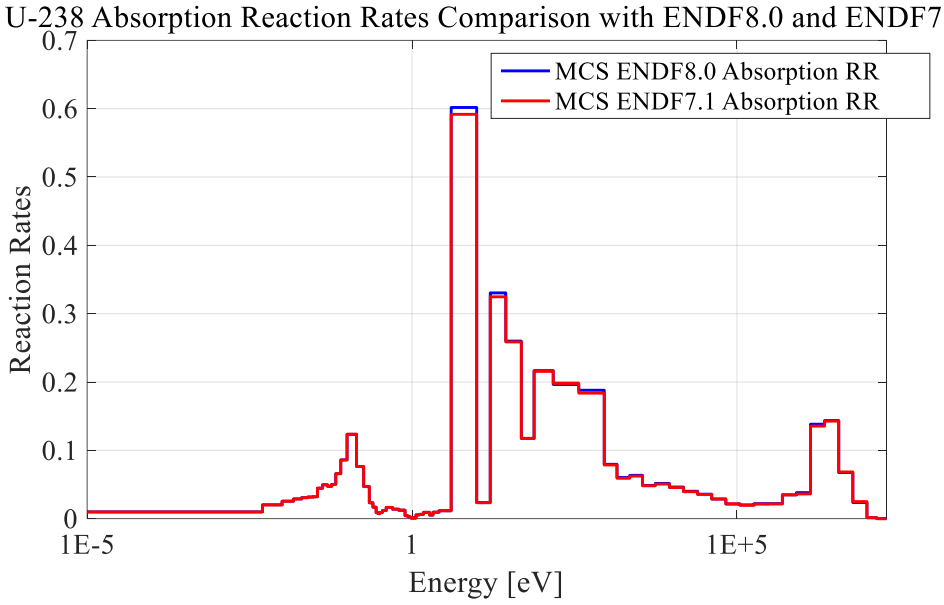

Figure 12. U-238 Absorption Reaction Rates Comparison of 4.9w/o fuel pin with ENDF/B-VIII.0 and ENDF/B-VII.1 in MCS

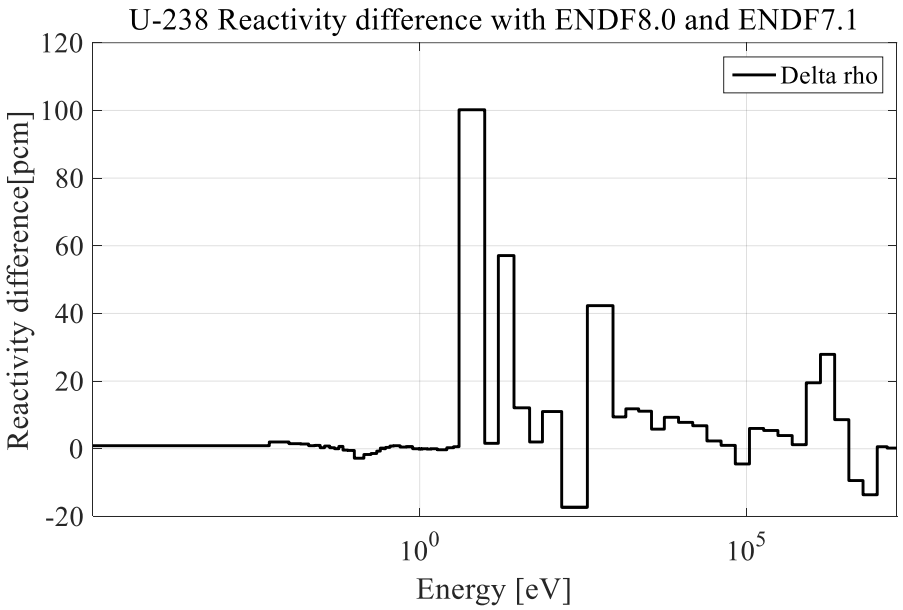

Figure 13. U-238 Reactivity difference of 4.9w/o fuel pin with ENDF/B-VIII.0 and ENDF/B-VII.1 in MCS

5.3. U-235 Total XS

Uranium 235 is the most important nuclide responsible for the Fission of nuclear fuel, and simulation results can respond sensitively to changes in Uranium 235 XS in ENDF version. As shown as Figure 15, U-235 XS difference between ENDF/B-VIII.0 and ENDF/B-VII.1 is within 5%. It is not the negligible difference value. In Figure 16, 17 & 18, Elastic XS, Fission XS and Thermal Scattering XS of U-235 has 9.6% XS difference of ENDF version as maximum. In principle, the thermal energy region of Elastic XS and thermal Scattering XS showed a noticeable decrease in influence within -7% difference.

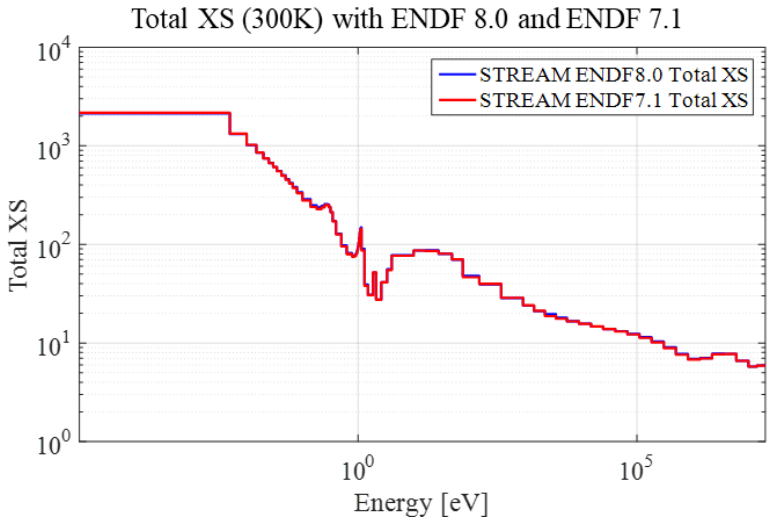

Figure 14. U-235 Total XS with ENDF/B-VIII.0 and ENDF/B-VII.1 at 300K

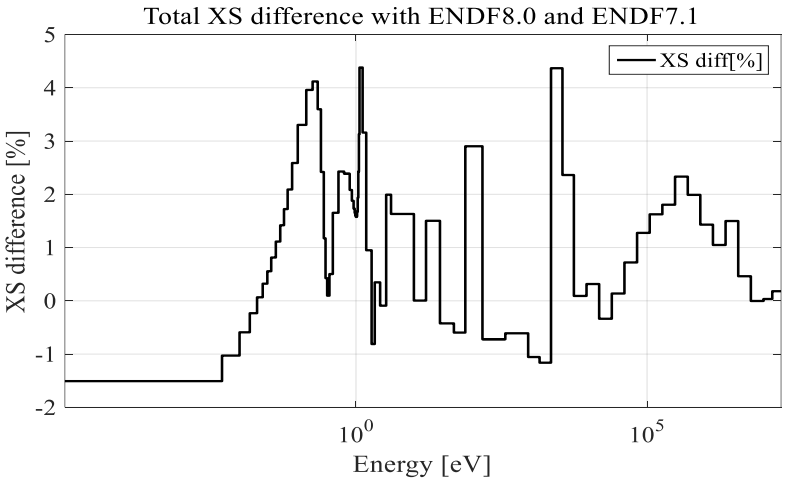

Figure 15. U-235 Total XS difference with ENDF/B-VIII.0 and ENDF/B-VII.1 at 300K

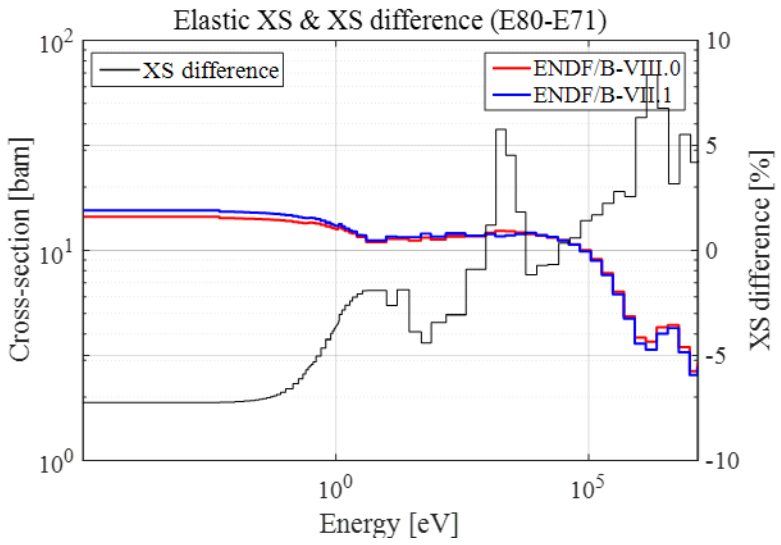

Figure 16. U-235 Elastic XS and XS difference with ENDF/B-VIII.0 and ENDF/B-VII.1 at 300K

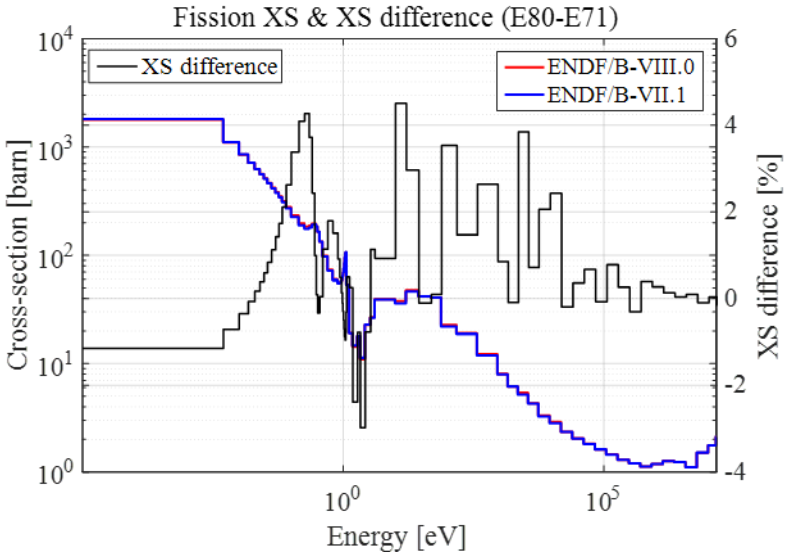

Figure 17. U-235 Fission XS and XS difference with ENDF/B-VIII.0 and ENDF/B-VII.1 at 300K

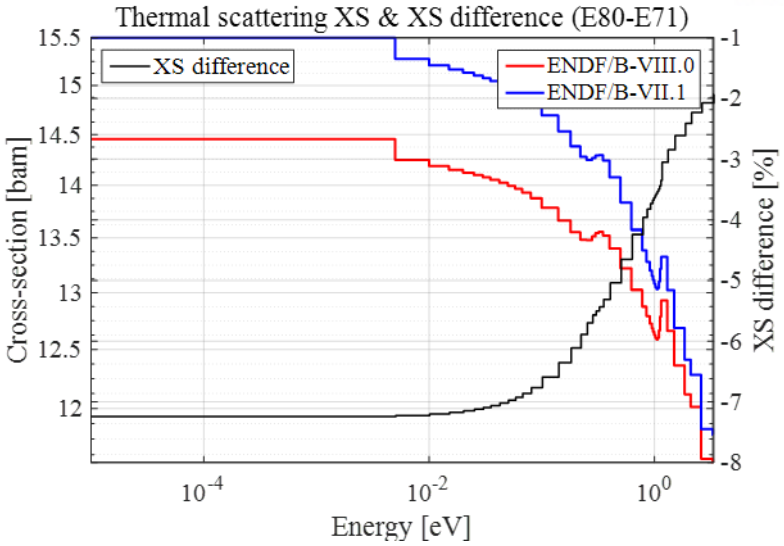

Figure 18. U-235 Thermal Scattering XS and XS difference with ENDF/B-VIII.0 and ENDF/B-VII.1 at 300K

5.4. U-235 Absorption Reaction Rates Comparison with ENDF/B-VIII.0 and ENDF/B-VII.1

5.4.1. STREAM – U-235 Absorption RR & Reactivity difference

As compare with U-235 absorption reaction rates and reactivity difference between ENDF/B-VIII.0 and ENDF/B-VII.1, 4.9% w/o NCA pin is used. Because fission XS of U-235 is bigger than other XSs and fission XS of thermal energy region below 3.3eV is increased in ENDF/B-VIII.0, Figure 20 shows U-235 Absorption reaction rates of ENDF/B-VIII.0 is increased with similar shape of U-235 Fission XS difference. Reactivity difference of each group between ENDF/B-VIII.0 and ENDF/B-VII.1 is within allowable range such as 100 pcm and total reactivity difference is about 279 pcm in STREAM.

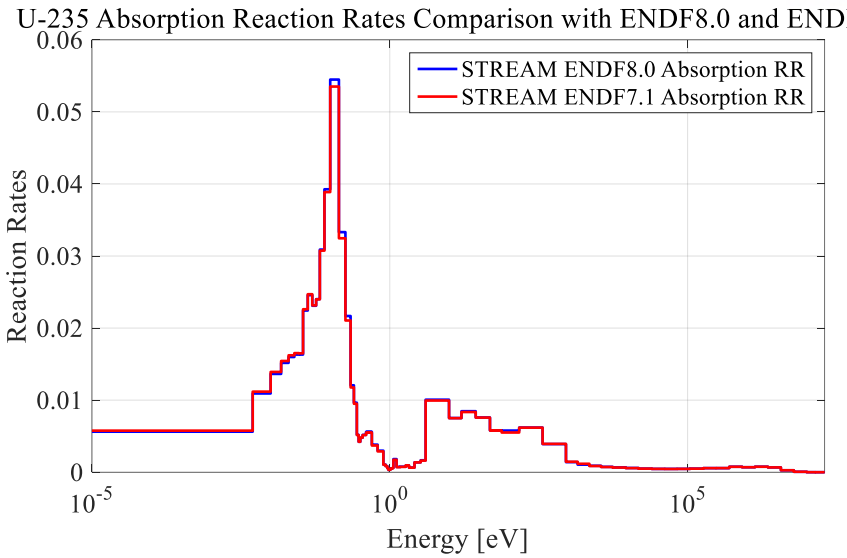

Figure 19. U-235 Absorption Reaction Rates Comparison of 4.9w/o fuel pin with ENDF/B-VIII.0 and ENDF/B-VII.1 in STREAM

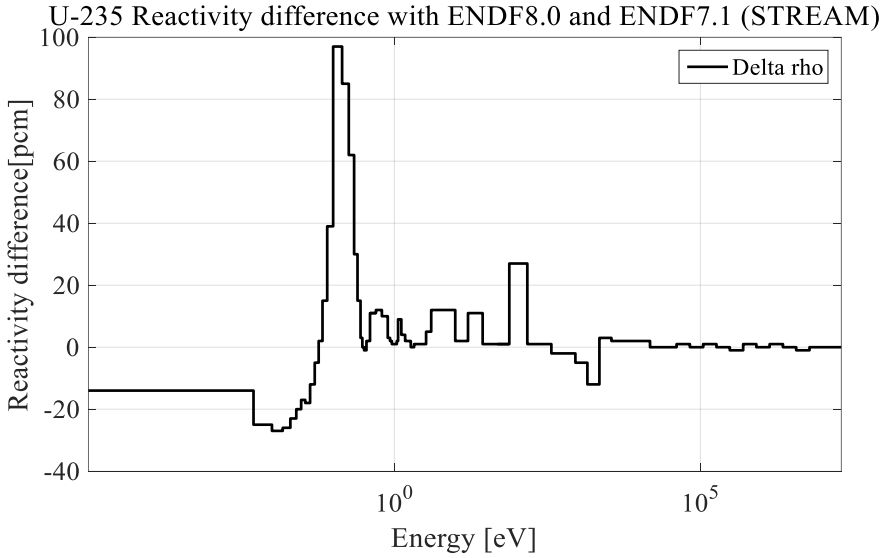

Figure 20. U-235 Reactivity difference of 4.9w/o fuel pin with ENDF/B-VIII.0 and ENDF/B-VII.1 in STREAM

5.4.2. MCS – U-235 Absorption RR & Reactivity difference

The Reactivity difference of MCS can be different with the reactivity difference of STREAM. The Figure 21 is tallied MCS absorption reaction rates value with STREAM 72 group energy boundary. Reactivity difference of each group between ENDF/B-VIII.0 and ENDF/B-VII.1 is

within allowable range such as 100 pcm and total reactivity difference is about 289 pcm in MCS. The shape of U-235 MCS Reactivity difference with ENDF/B-VIII.0 and ENDF/B-VII.1 is very similar with the shape of U-235 STREAM Reactivity difference.

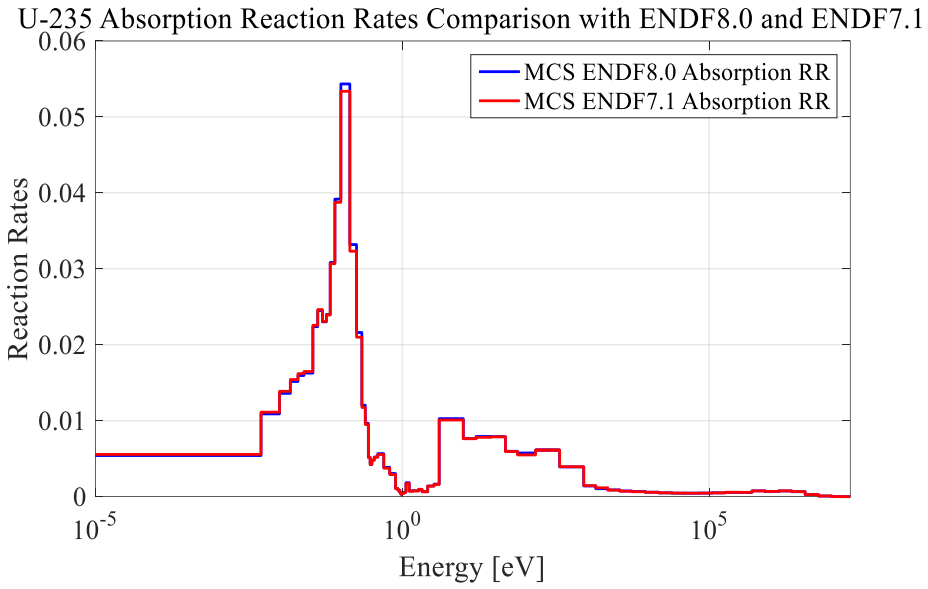

Figure 21. U-235 Absorption Reaction Rates Comparison of 4.9w/o fuel pin with ENDF/B-VIII.0 and ENDF/B-VII.1 in MCS

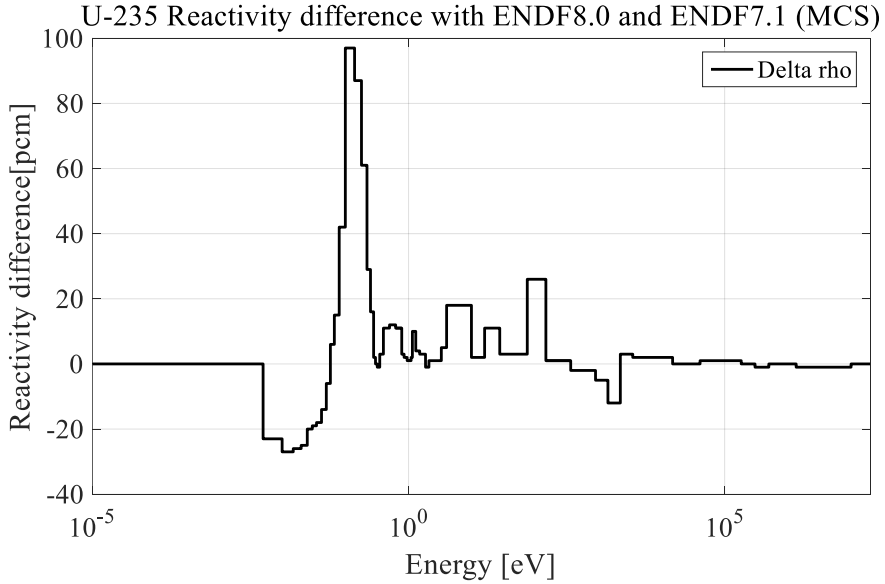

Figure 22. U-235 Reactivity difference of 4.9w/o fuel pin with ENDF/B-VIII.0 and ENDF/B-VII.1 in MCS

VI. XS COMPARISON OF MAJOR ISOTOPES

In this chapter, the XSs of important nuclei between ENDF/B-VIII.0 and ENDF/B-VII.1 except uranium has compared as STREAM 72 group energy structure.

The nuclides to be compared are: ^{1}H, light water(HinH2O), polyethylene(HinCH2), ^{4}He, ^{12,13}C, ^{16}O, ^{54,56,57,58}Fe, $^{58-62,64}$Ni, $^{182-186}$W

On the XS figures, ENDF format of each XS is represented. The description of mf 3 is Reaction cross sections. The meaning of mt 1 is (n,total); Neutron total cross sections. The meaning of mt 2 is (z,z0); Elastic scattering cross section for incident particles. The meaning of mt 221 is the generated XS matrix; it was given Thermal scattering XS by NJOY program.

6.1. 1-H-1 ENDF/B-VIII.0 & ENDF/B-VII.1 XS difference (293.6K)

In reactor simulations, the XS of hydrogen is not used in itself but is used through s(a,b) calculations. However, since it is one of the most important nuclides, it was calculated and compared. Total XS difference is within 0.6% at the fast energy region and most of the difference comes from elastic XS difference.

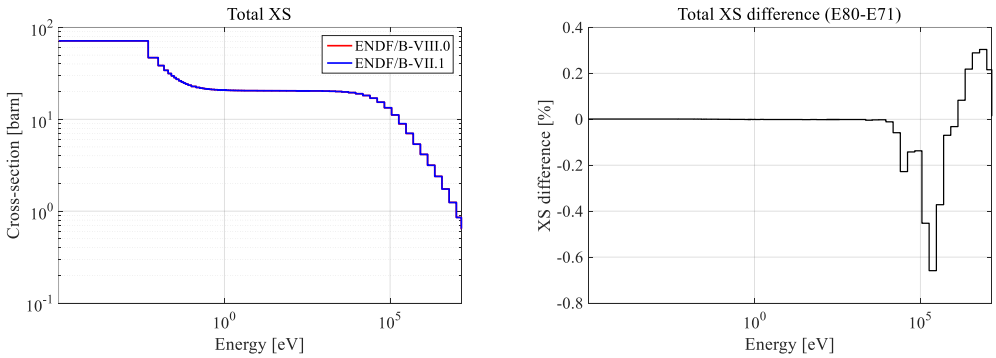

Figure 23. H-1 Total XS and XS difference with ENDF/B-VIII.0 and ENDF/B-VII.1 at 293.6K

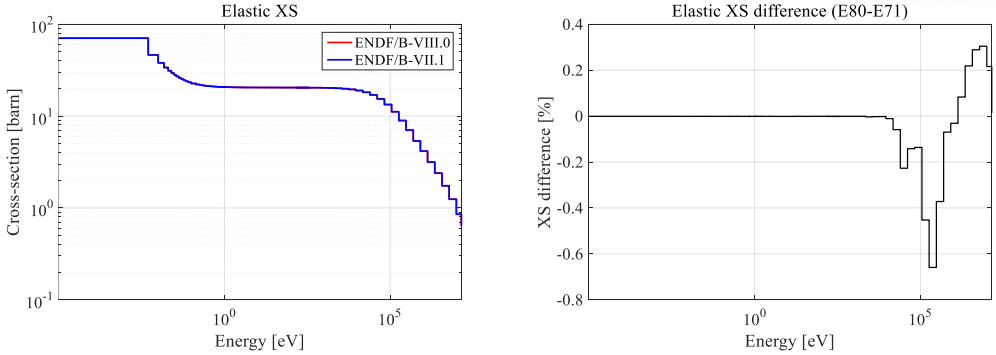

Figure 24. H-1 Elastic XS and XS difference with ENDF/B-VIII.0 and ENDF/B-VII.1 at 293.6K

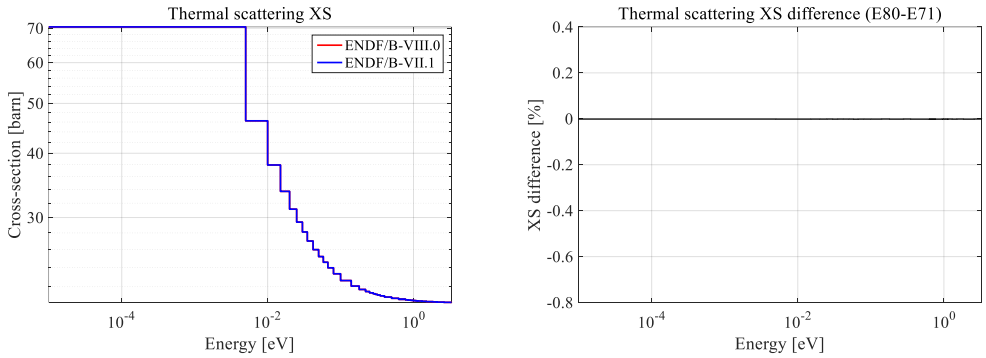

Figure 25. H-1 Thermal scattering XS and XS difference with ENDF/B-VIII.0 and ENDF/B-VII.1 at 293.6K

6.2. 1-HinH2O-1 ENDF/B-VIII.0 & ENDF/B-VII.1 XS difference (293.6K)

The cross-sections for hydrogen in water has calculated with neutron cross-section library and thermal scattering library of ENDF versions. The thermal cross-section for hydrogen in water is different from XSs of hydrogen. Thermal scattering XS difference of hydrogen in water has increased within 2.7% at the total energy region than thermal scattering XS difference of normal hydrogen, and it tends to get smaller in the resonance energy region.

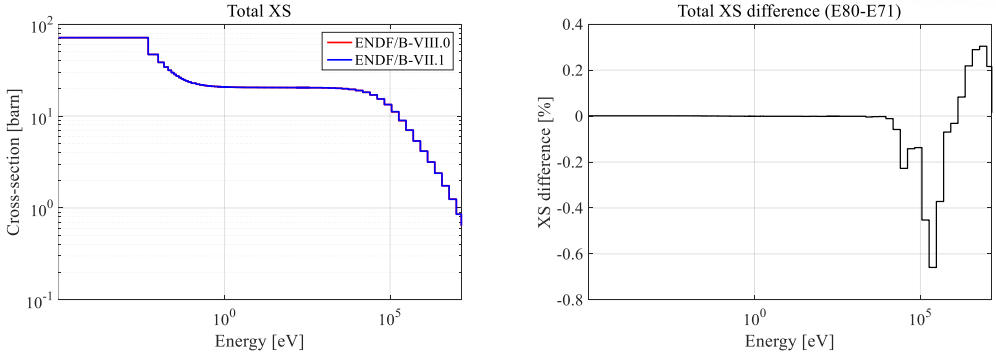

Figure 26. HinH2O Total XS and XS difference with ENDF/B-VIII.0 and ENDF/B-VII.1 at 293.6K

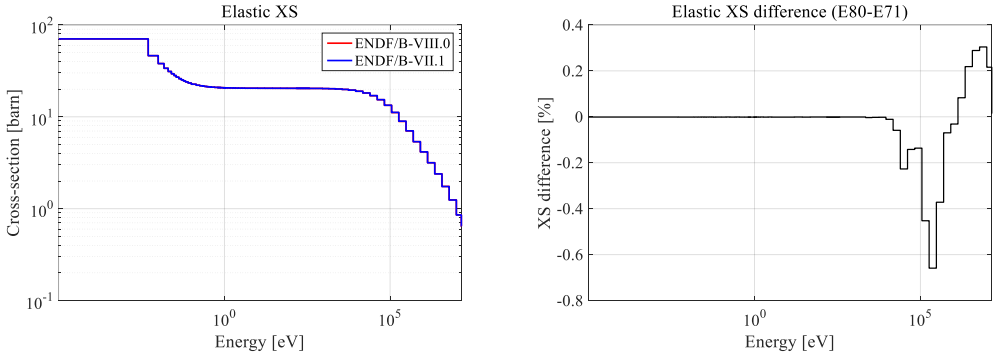

Figure 27. HinH2O Elastic XS and XS difference with ENDF/B-VIII.0 and ENDF/B-VII.1 at 293.6K

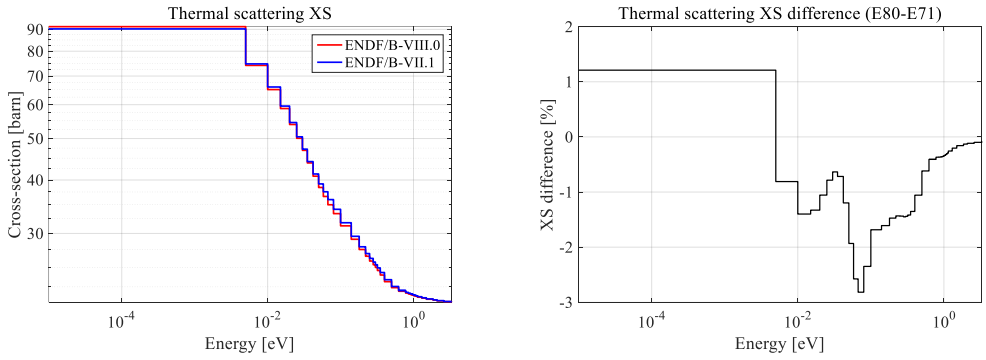

Figure 28. HinH2O Thermal scattering XS and XS difference with ENDF/B-VIII.0 and ENDF/B-VII.1 at 293.6K

6.3. 1-HinCH2-1 ENDF/B-VIII.0 & ENDF/B-VII.1 XS difference (293.6K)

Hydrogen in polyethylene usually tends to be used within fast reactor simulation. Compared to

the XSs of hydrogen, thermal scattering XS of hydrogen in polyethylene is reduced. In the under 4eV energy region, thermal scattering XS of hydrogen in polyethylene from ENDF/B-VIII.0 has been reduced by -15% than its of ENDF/B-VII.1.

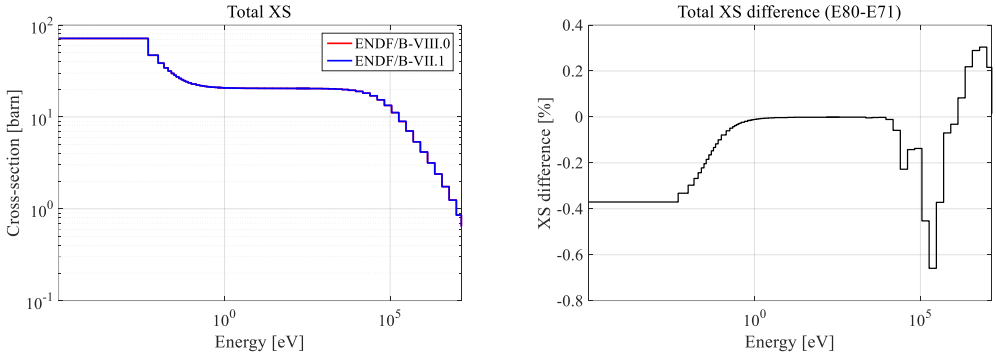

Figure 29. HinCH2 Total XS and XS difference with ENDF/B-VIII.0 and ENDF/B-VII.1 at 293.6K

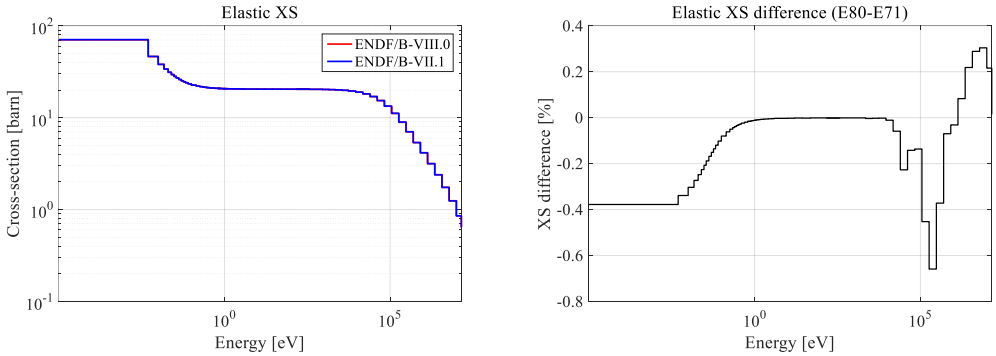

Figure 30. HinCH2 Elastic XS and XS difference with ENDF/B-VIII.0 and ENDF/B-VII.1 at 293.6K

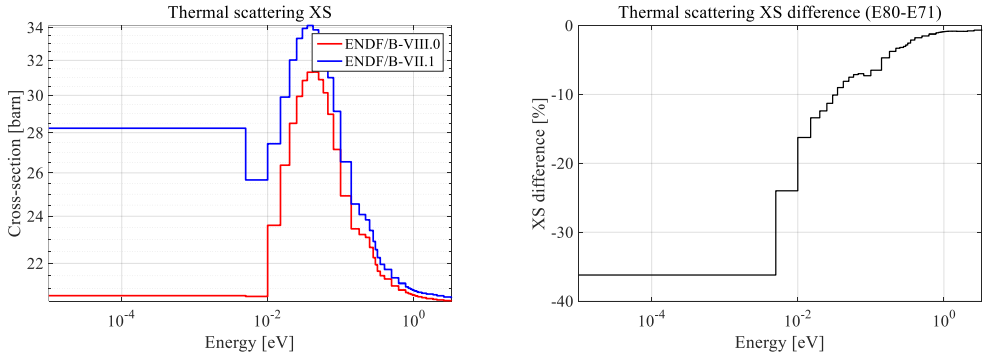

Figure 31. HinCH2 Thermal scattering XS and XS difference with ENDF/B-VIII.0 and ENDF/B-VII.1 at 293.6K

6.4. 2-He-4 ENDF/B-VIII.0 & ENDF/B-VII.1 XS difference (293.6K)

The XS of Helium has no difference between ENDF/B-VIII.0 and ENDF/B-VII.1 library versions.

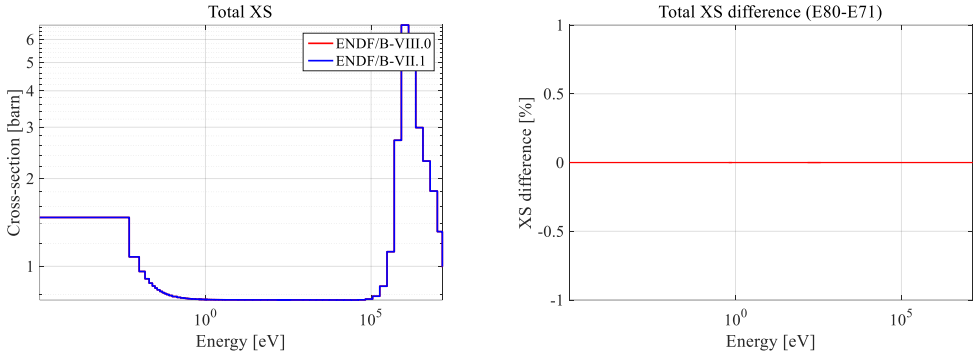

Figure 32. He-4 Total XS and XS difference with ENDF/B-VIII.0 and ENDF/B-VII.1 at 293.6K

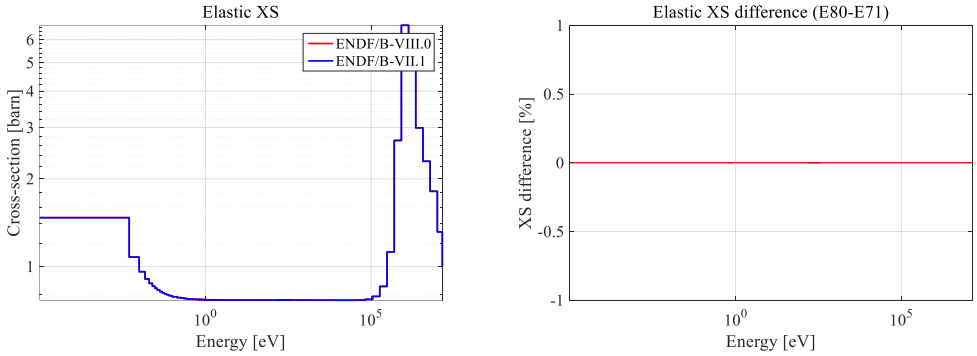

Figure 33. He-4 Elastic XS and XS difference with ENDF/B-VIII.0 and ENDF/B-VII.1 at 293.6K

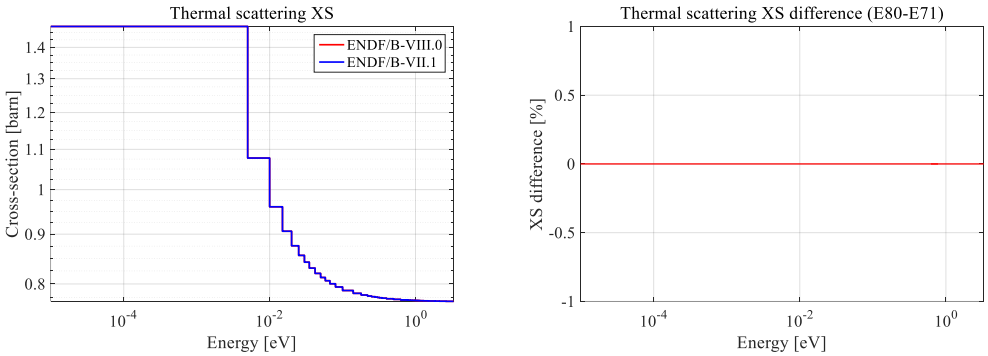

Figure 34. He-4 Thermal scattering XS and XS difference with ENDF/B-VIII.0 and ENDF/B-VII.1 at 293.6K

6.5. 6-C-12 ENDF/B-VIII.0 & ENDF/B-VII.1 XS difference (293.6K)

The ENDF/B-VIII.0 release is the first ENDF/B release to include ^{12}C(98.9%) and ^{13}C(1.1%) isotopic evaluations in lieu of a natural carbon evaluation. Direct XS comparison with ^{12}C of ENDF/B-VIII.0 and ^{nat}C of ENDF/B-VII.1 can be inaccurate. It can shows the maximum 1.62% increase at fast energy region, but it can be negligible.

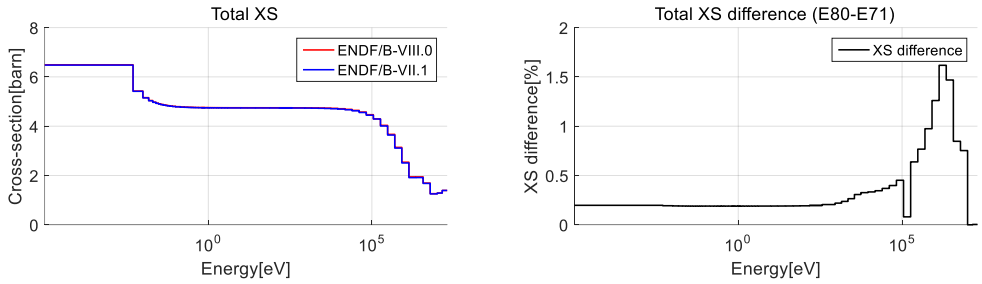

Figure 35. C-12 Total XS and XS difference with ENDF/B-VIII.0 and ENDF/B-VII.1 at 293.6K

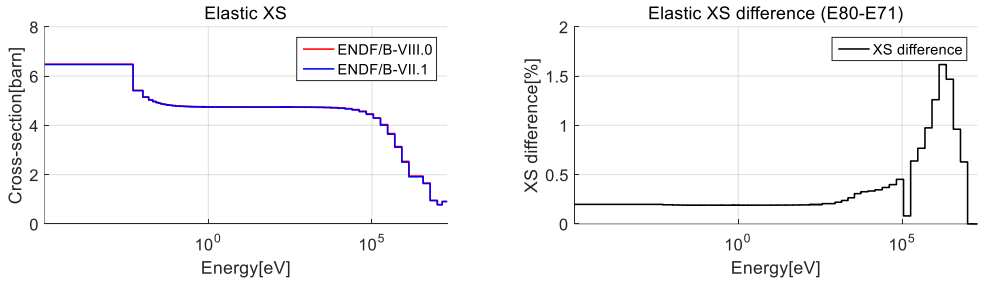

Figure 36. C-12 Elastic XS and XS difference with ENDF/B-VIII.0 and ENDF/B-VII.1 at 293.6K

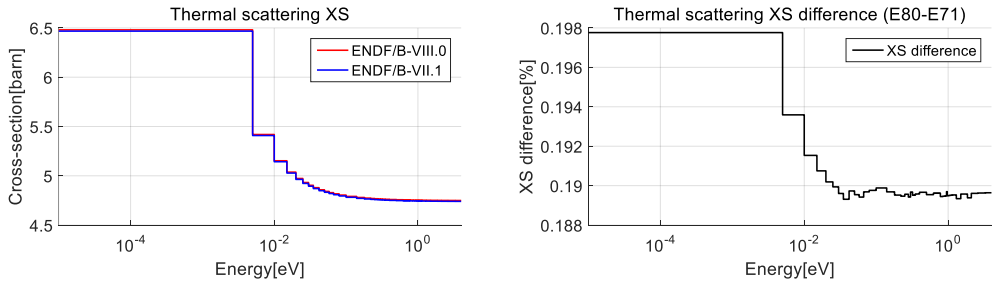

Figure 37. C-12 Thermal scattering XS and XS difference with ENDF/B-VIII.0 and ENDF/B-VII.1 at 293.6K

6.6. 8-O-16 ENDF/B-VIII.0 & ENDF/B-VII.1 XS difference (293.6K)

From 7 MeV and above, the Oxigen XS of ENDF/B-VIII.0 was deliberately harmonized smoothly with the existing XS of ENDF/B-VII.0, and from energy above 9 MeV, the capture XS of ENDF/B-VIII.0 was identical to the existing ENDF/B-VII.1. Compared to ENDF/B-VII.1 total XS of ^{16}O, ENDF/B-VIII.0 total XS of ^{16}O tended to decrease by 1.4% overall except for Fast region, and increased by nearly 4% in Fast region. In the thermal region, it decreased by 1.5% over the whole range.

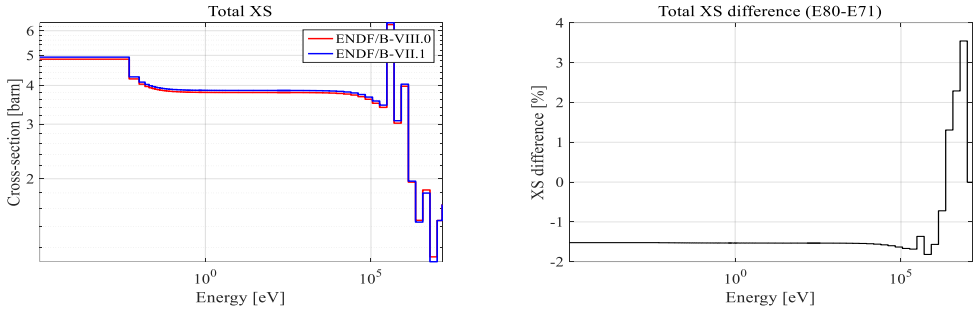

Figure 38. O-16 Total XS and XS difference with ENDF/B-VIII.0 and ENDF/B-VII.1 at 293.6K

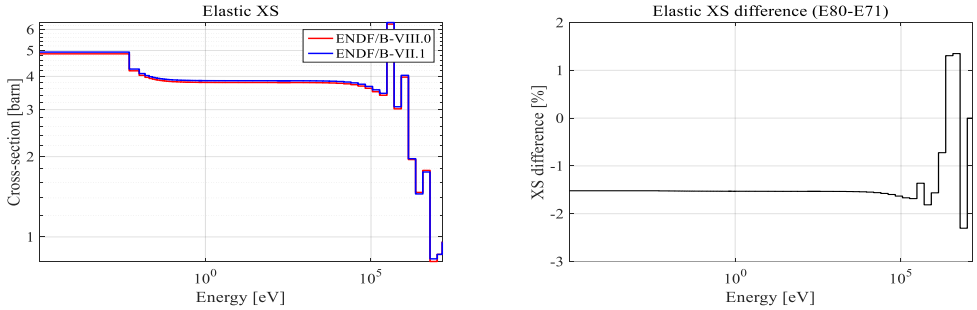

Figure 39. O-16 Elastic XS and XS difference with ENDF/B-VIII.0 and ENDF/B-VII.1 at 293.6K

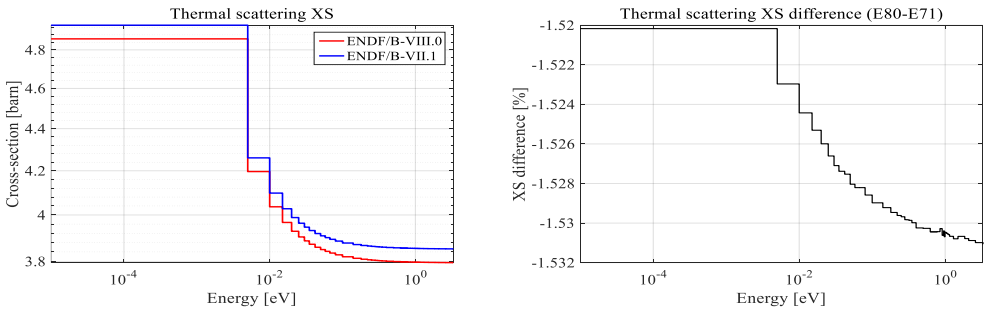

Figure 40. O-16 Thermal scattering XS and XS difference with ENDF/B-VIII.0 and ENDF/B-VII.1 at 293.6K

6.7. 26-Fe-54 ENDF/B-VIII.0 & ENDF/B-VII.1 XS difference (293.6K)

Although ^{56}Fe is the dominant iron isotope, ^{54,57,58}Fe also has a significant contribution. As shown as Figure 41, in the total XS of ^{54}Fe, the XS difference moves up and down until 10% difference between 2.23945keV to 5.53000keV. At this difference, Elastic XS is dominant. Additionally, the highest resonance energy range and resonance amplitude of ^{54}Fe is wider than previous version as Figure 44.

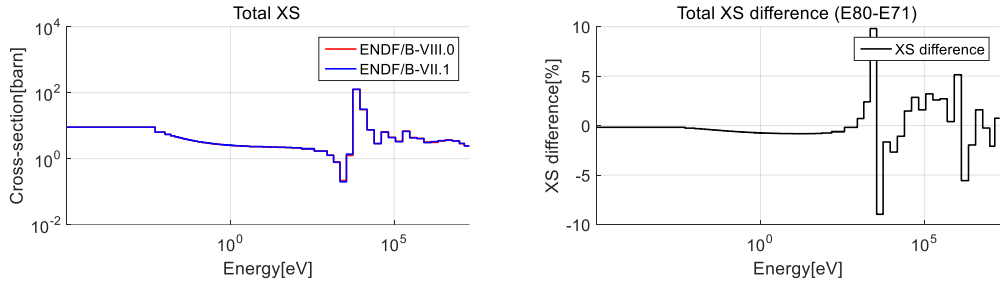

Figure 41. Fe-54 Total XS and XS difference with ENDF/B-VIII.0 and ENDF/B-VII.1 at 293.6K

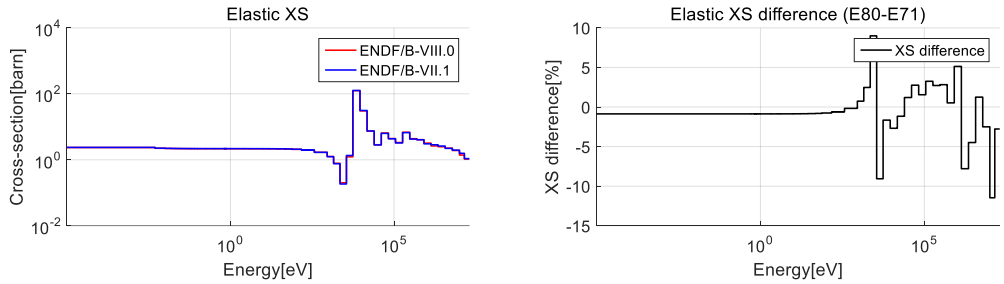

Figure 42. Fe-54 Elastic XS and XS difference with ENDF/B-VIII.0 and ENDF/B-VII.1 at 293.6K

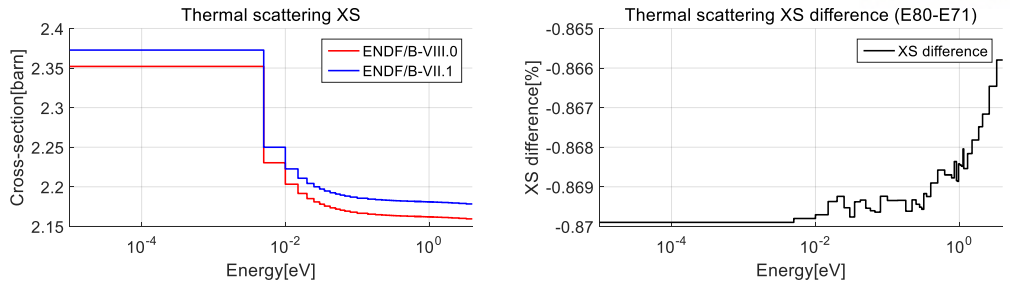

Figure 43. Fe-54 Thermal scattering XS and XS difference with ENDF/B-VIII.0 and ENDF/B-VII.1 at 293.6K

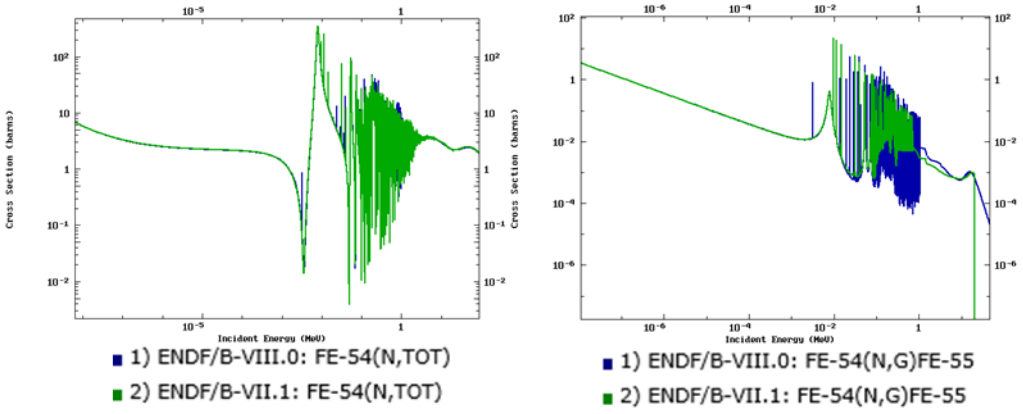

Figure 44. Fe-54 Total XS and Radiative capture XS with ENDF/B-VIII.0 and ENDF/B-VII.1

6.8. 26-Fe-56 ENDF/B-VIII.0 & ENDF/B-VII.1 XS difference (293.6K)

^{56}Fe is the dominant isotope with a natural abundance of 91.8%. Therefore, ^{56}Fe is the main focus of the CIELO iron project. Resonance region has been changed very much, and at the capture XS, about 0.25% of background is increased in a whole region. Unlike ^{54}Fe, the response energy region has not increased, there is an increase of the inelastic cross section area on ^{56}Fe.

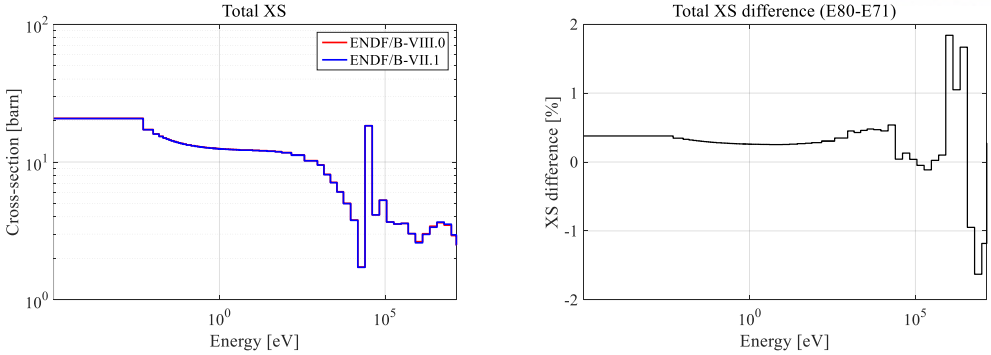

Figure 45. Fe-56 Total XS and XS difference with ENDF/B-VIII.0 and ENDF/B-VII.1 at 293.6K

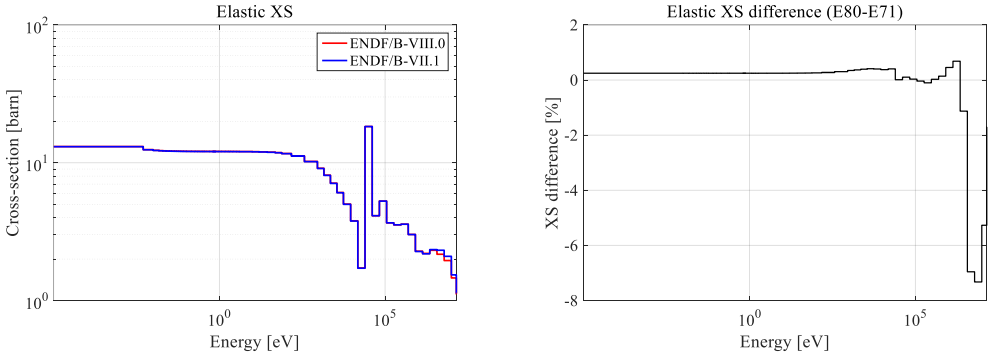

Figure 46. Fe-56 Elastic XS and XS difference with ENDF/B-VIII.0 and ENDF/B-VII.1 at 293.6K

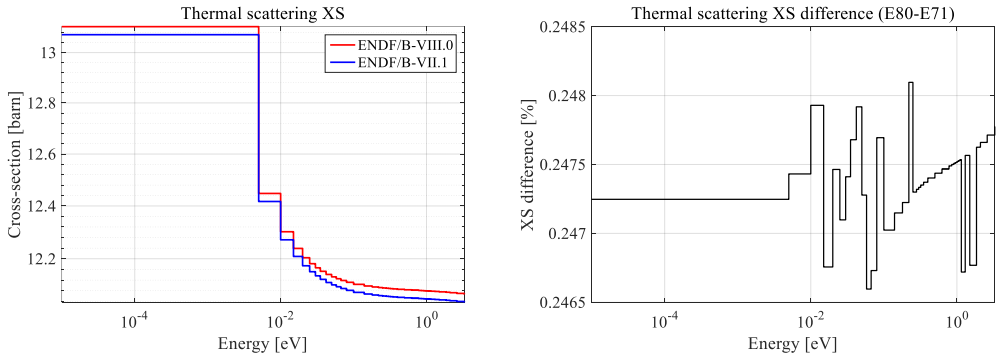

Figure 47. Fe-56 Thermal scattering XS and XS difference with ENDF/B-VIII.0 and ENDF/B-VII.1 at 293.6K

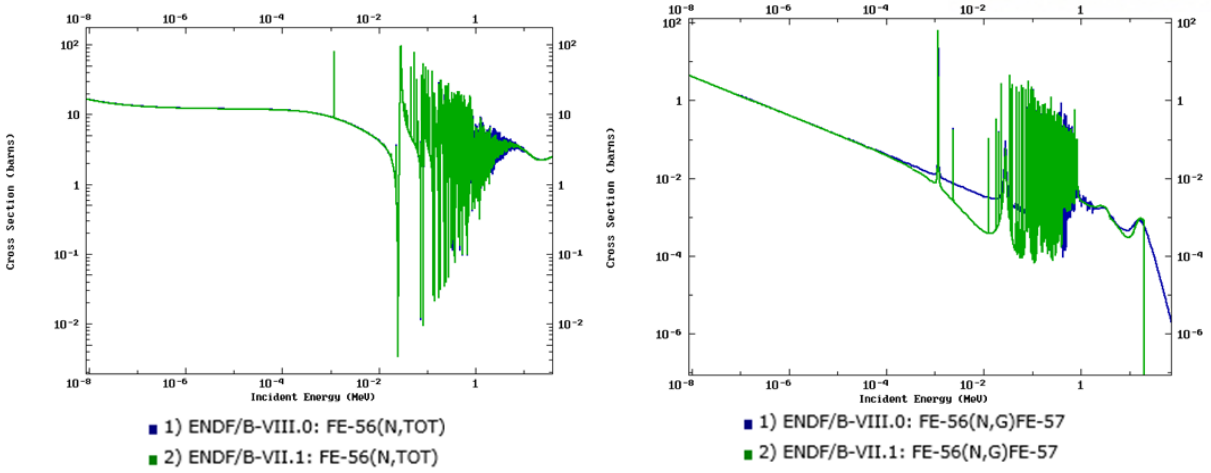

Figure 48. Fe-56 Total XS and Radiative capture XS with ENDF/B-VIII.0 and ENDF/B-VII.1

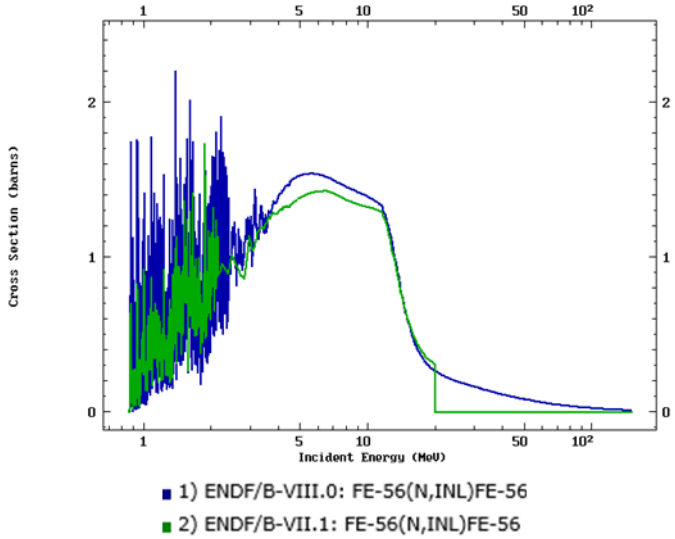

Figure 49. Fe-56 Inelastic XS with ENDF/B-VIII.0 and ENDF/B-VII.1

6.9. 26-Fe-57 ENDF/B-VIII.0 & ENDF/B-VII.1 XS difference (293.6K)

Although ^{56}Fe is the dominant iron isotope, ^{54,57,58}Fe also has a significant contribution. In Figure 50 and 53, a very big XS difference is represented. In the thermal energy region and resonance energy region below the 1.4251keV, XS difference from maximum -90% to minimum -20% is represented. Also in the thermal scattering XS of ^{57}Fe, significant change ~76.8% decrease is shown.

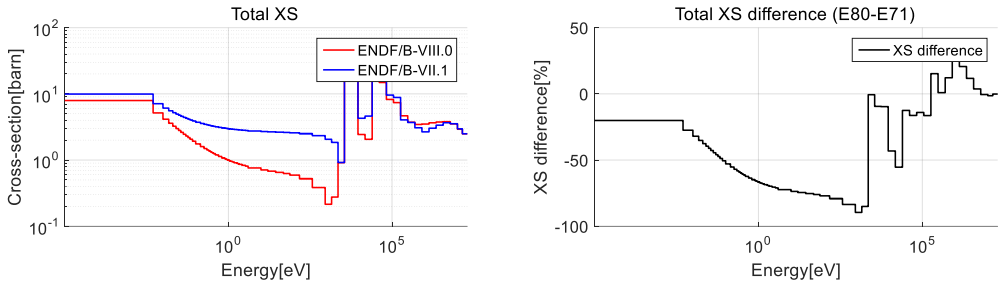

Figure 50. Fe-57 Total XS and XS difference with ENDF/B-VIII.0 and ENDF/B-VII.1 at 293.6K

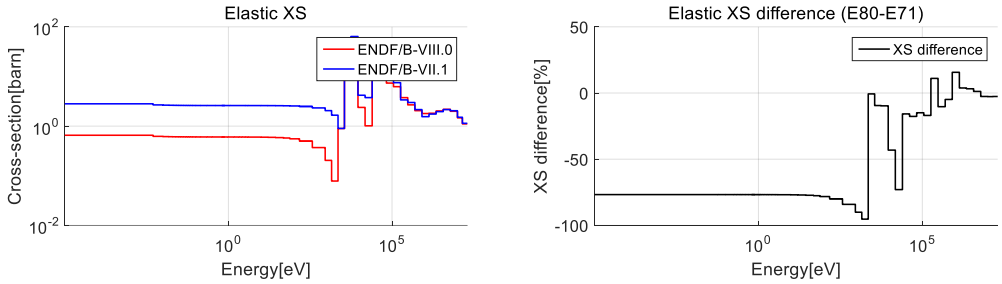

Figure 51. Fe-57 Elastic XS and XS difference with ENDF/B-VIII.0 and ENDF/B-VII.1 at 293.6K

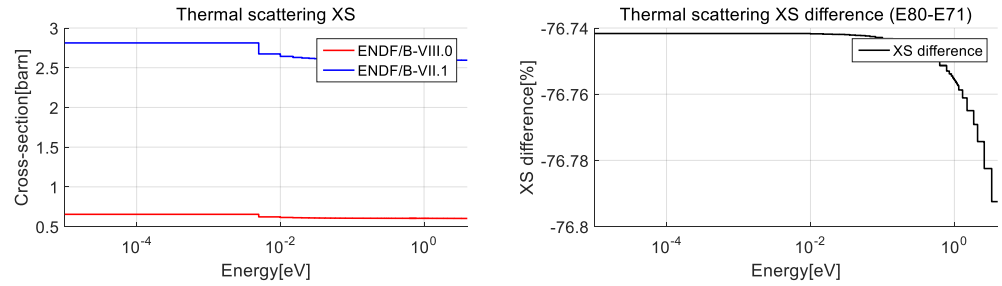

Figure 52. Fe-57 Thermal scattering XS and XS difference with ENDF/B-VIII.0 and ENDF/B-VII.1 at 293.6K

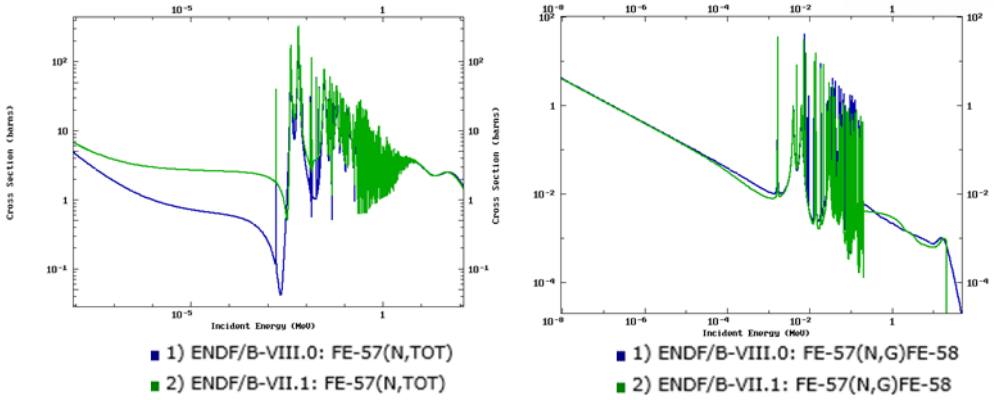

Figure 53. Fe-57 Total XS and Radiative capture XS with ENDF/B-VIII.0 and ENDF/B-VII.1

6.10. 26-Fe-58 ENDF/B-VIII.0 & ENDF/B-VII.1 XS difference (293.6K)

Although ^{56}Fe is the dominant iron isotope, ^{54,57,58}Fe also has a significant contribution. The largest variation of total XS in iron atoms is on ^{58}Fe. Up to 140% increase than previous version, and total XS tends to increase in most energy group areas. Both of Elastic XS and Thermal scattering XS are increased significantly also. The resonance amplitude of capture XS is wider than previous version as Figure 57.

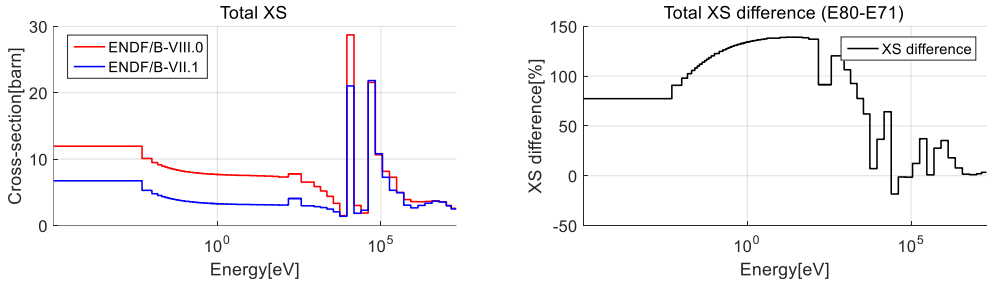

Figure 54. Fe-58 Total XS and XS difference with ENDF/B-VIII.0 and ENDF/B-VII.1 at 293.6K

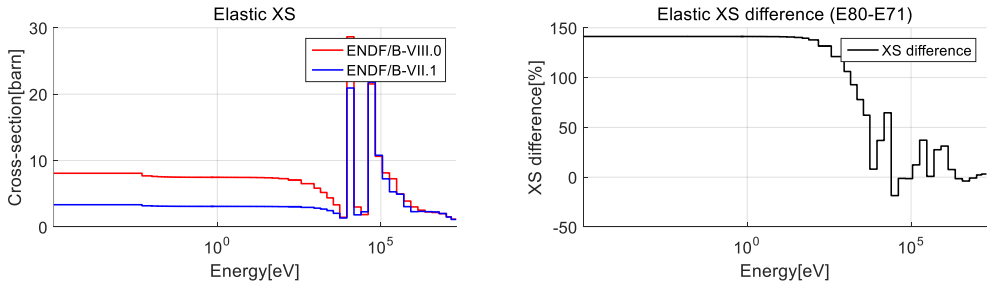

Figure 55. Fe-58 Elastic XS and XS difference with ENDF/B-VIII.0 and ENDF/B-VII.1 at 293.6K

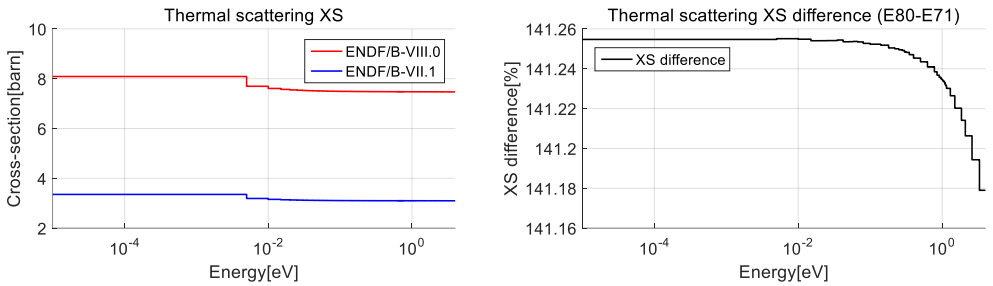

Figure 56. Fe-58 Thermal scattering XS and XS difference with ENDF/B-VIII.0 and ENDF/B-VII.1 at 293.6K

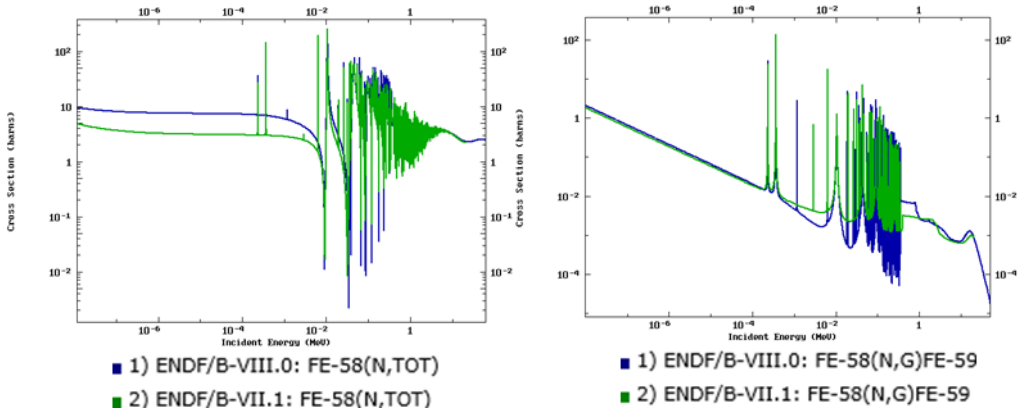

Figure 57. Fe-58 Total XS and Radiative capture XS with ENDF/B-VIII.0 and ENDF/B-VII.1

6.11. 28-Ni-58 ENDF/B-VIII.0 & ENDF/B-VII.1 XS difference (293.6K)

In the ENDF/B-VIII.0, ^{58}Ni is changed at alpha particle production cross section and resonance region range, but not noticeable.

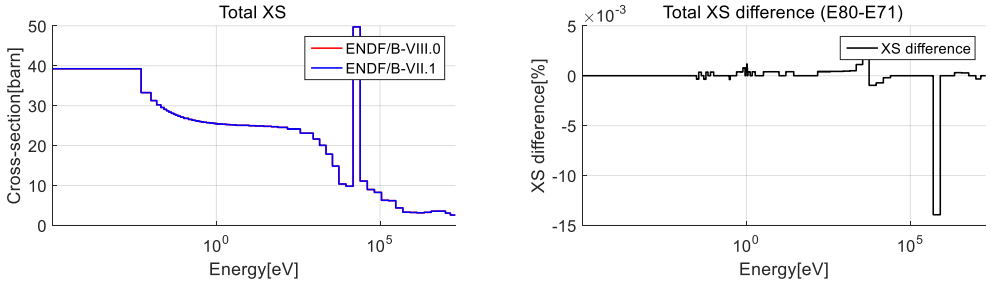

Figure 58. Ni-58 Total XS and XS difference with ENDF/B-VIII.0 and ENDF/B-VII.1 at 293.6K

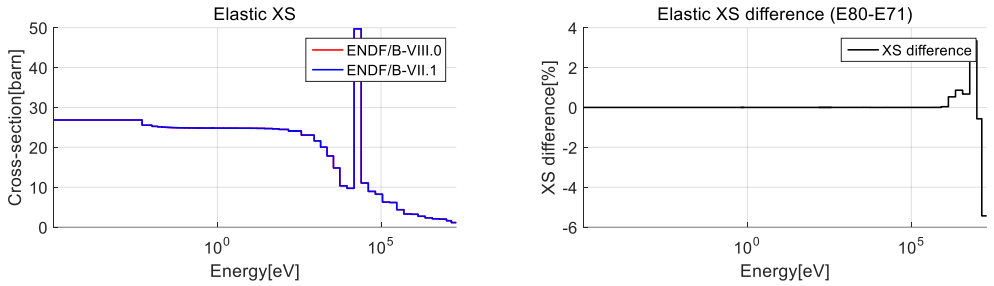

Figure 59. Ni-58 Elastic XS and XS difference with ENDF/B-VIII.0 and ENDF/B-VII.1 at 293.6K

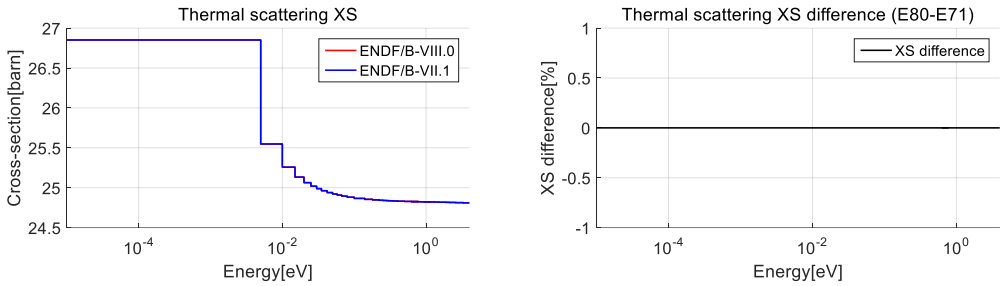

Figure 60. Ni-58 Thermal scattering XS and XS difference with ENDF/B-VIII.0 and ENDF/B-VII.1 at 293.6K

6.12. 28-Ni-60 ENDF/B-VIII.0 & ENDF/B-VII.1 XS difference (293.6K)

In the ENDF/B-VIII.0, ^{60}Ni is changed at alpha particle production cross section and resonance region range, but not noticeable.

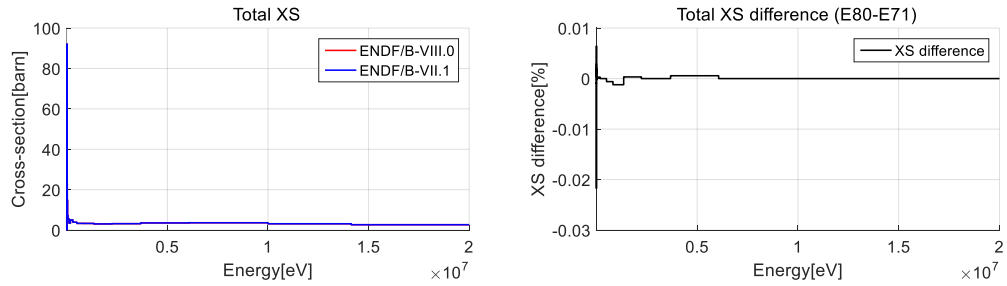

Figure 61. Ni-60 Total XS and XS difference with ENDF/B-VIII.0 and ENDF/B-VII.1 at 293.6K

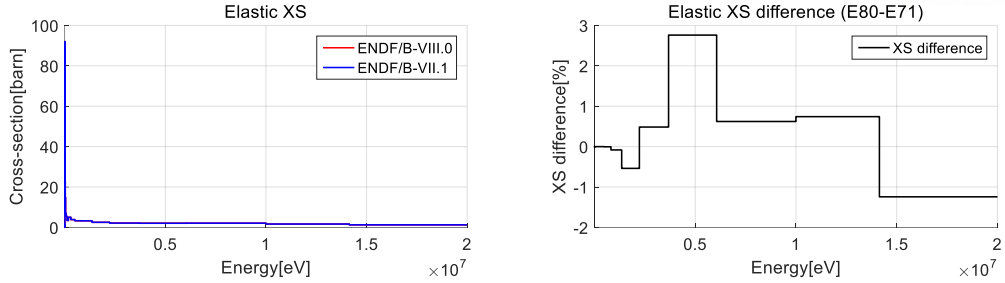

Figure 62. Ni-60 Elastic XS and XS difference with ENDF/B-VIII.0 and ENDF/B-VII.1 at 293.6K

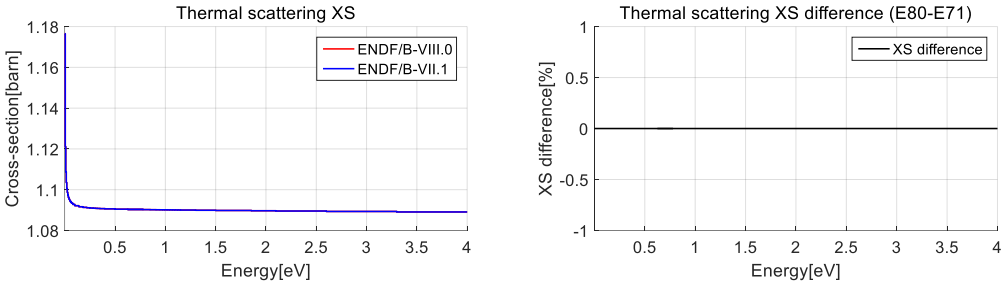

Figure 63. Ni-60 Thermal scattering XS and XS difference with ENDF/B-VIII.0 and ENDF/B-VII.1 at 293.6K

6.13. 28-Ni-61 ENDF/B-VIII.0 & ENDF/B-VII.1 XS difference (293.6K)

In the fast region of ^{61}Ni, Total XS and Elastic XS of ENDF/B-VIII.0 is increased under 50% more than ENDF/B-VII.1.

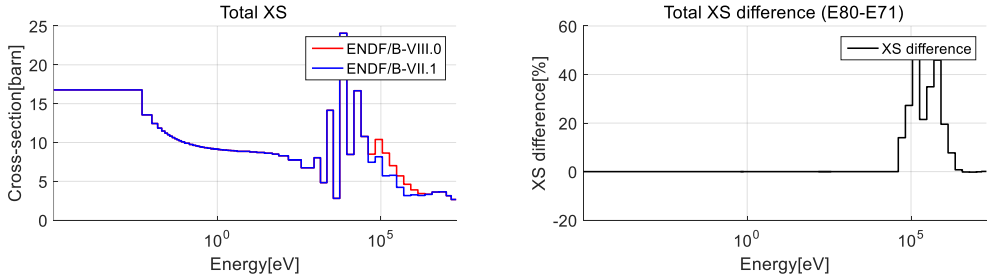

Figure 64. Ni-61 Total XS and XS difference with ENDF/B-VIII.0 and ENDF/B-VII.1 at 293.6K

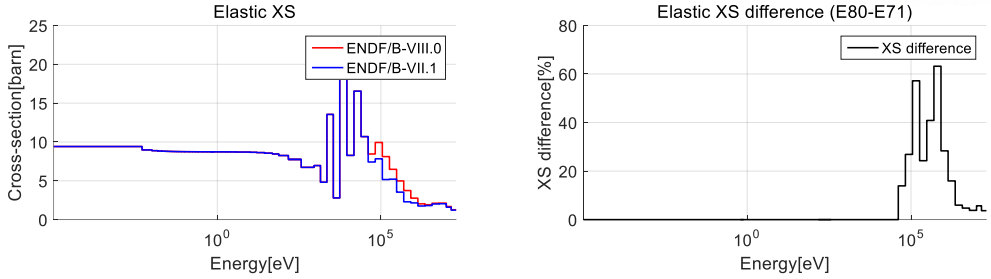

Figure 65. Ni-61 Elastic XS and XS difference with ENDF/B-VIII.0 and ENDF/B-VII.1 at 293.6K

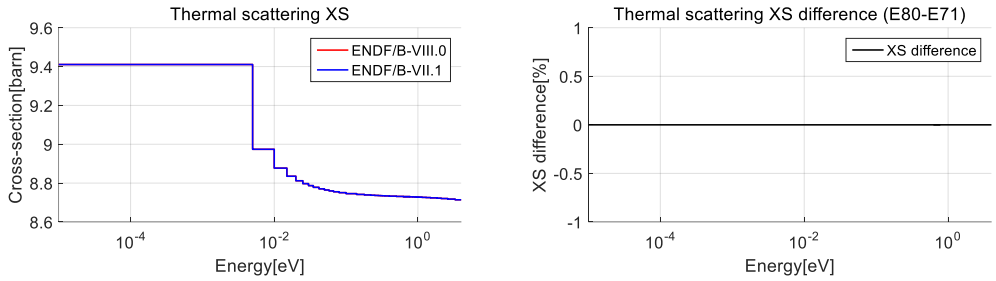

Figure 66. Ni-61 Thermal scattering XS and XS difference with ENDF/B-VIII.0 and ENDF/B-VII.1 at 293.6K

6.14. 28-Ni-62 ENDF/B-VIII.0 & ENDF/B-VII.1 XS difference (293.6K)

In the fast energy region over 6.065MeV, Elastic XS of ^{62}Ni is increased ~8%, but because XS value is too small, it is not noticeable.

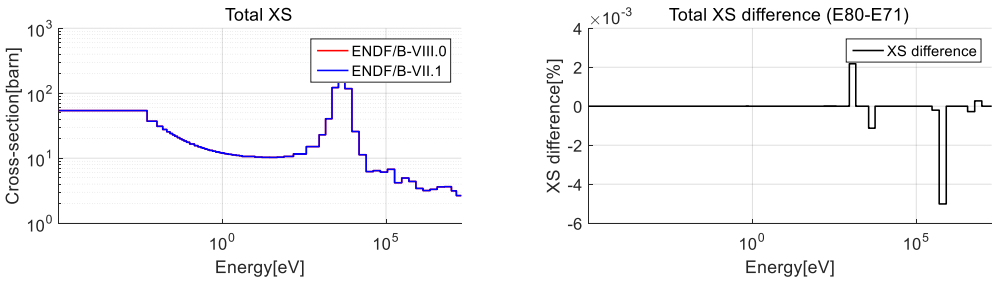

Figure 67. Ni-62 Total XS and XS difference with ENDF/B-VIII.0 and ENDF/B-VII.1 at 293.6K

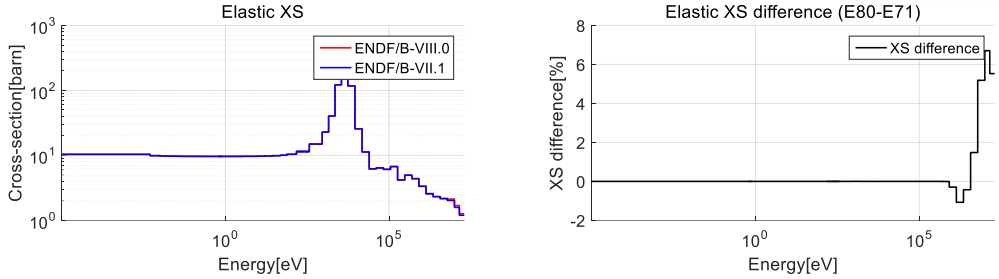

Figure 68. Ni-62 Elastic XS and XS difference with ENDF/B-VIII.0 and ENDF/B-VII.1 at 293.6K

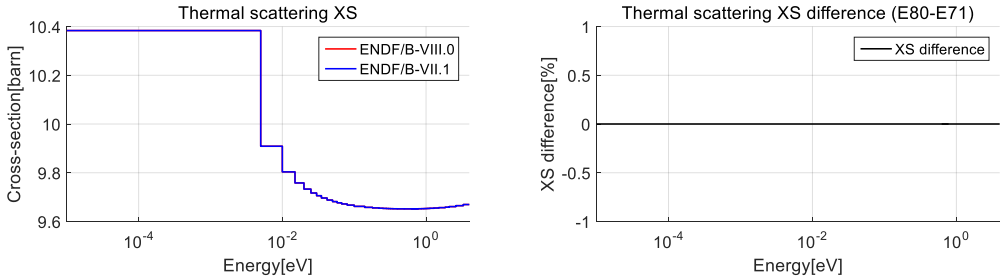

Figure 69. Ni-62 Thermal scattering XS and XS difference with ENDF/B-VIII.0 and ENDF/B-VII.1 at 293.6K

6.15. 28-Ni-64 ENDF/B-VIII.0 & ENDF/B-VII.1 XS difference (293.6K)

In the fast energy region over 6.065MeV, Elastic XS of ^{64}Ni is increased ~7%, but because XS value is too small, it is not noticeable.

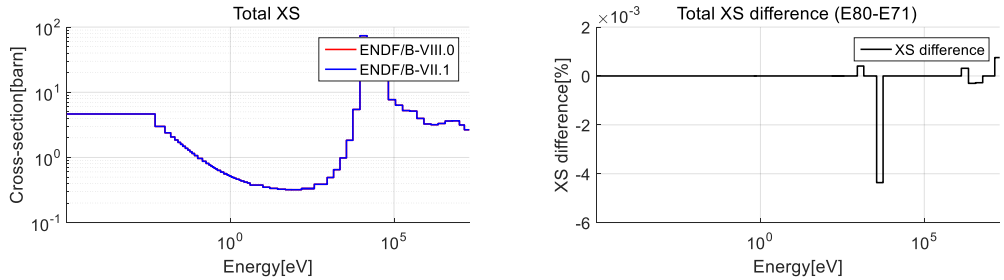

Figure 70. Ni-64 Total XS and XS difference with ENDF/B-VIII.0 and ENDF/B-VII.1 at 293.6K

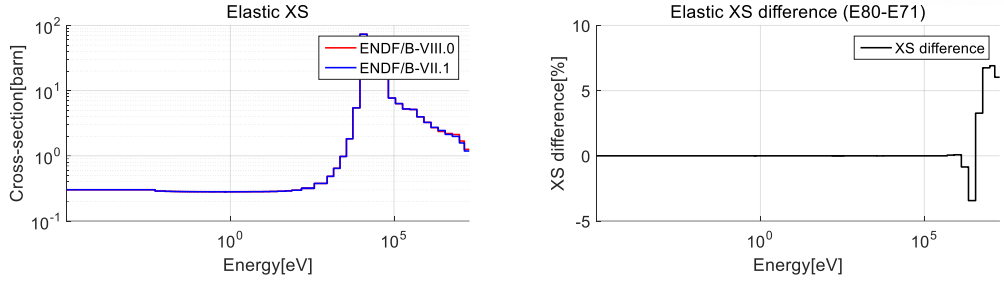

Figure 71. Ni-64 Elastic XS and XS difference with ENDF/B-VIII.0 and ENDF/B-VII.1 at 293.6K

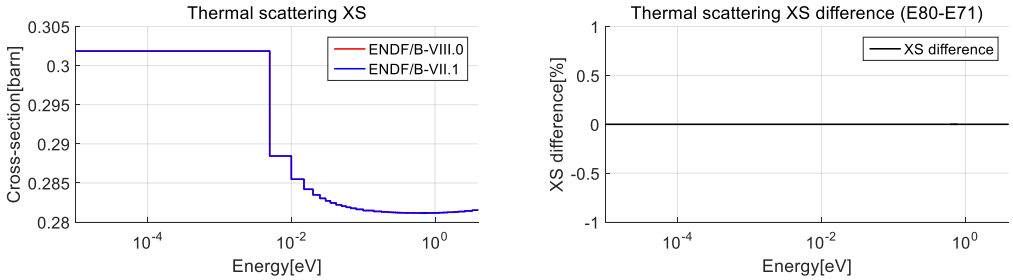

Figure 72. Ni-64 Thermal scattering XS and XS difference with ENDF/B-VIII.0 and ENDF/B-VII.1 at 293.6K

6.16. 74-W-182 ENDF/B-VIII.0 & ENDF/B-VII.1 XS difference (293.6K)

Tungsten is a structural material in many high-temperature nuclear applications including fusion systems. In ENDF/B-VII.1, $^{182-186}$W were extensively updated. The focus of this evaluation was the fast region and some minor adjustments were made to $^{182-186}$W resonance. In the ENDF/B-VIII.0 library evaluation, the resonance region of ^{182}W has been further expanded. In the ENDF/B-VII.1 library released, the resonance region of ^{182}W were extended to 4.5 keV, and now in the ENDF/B-VIII.0 library released, the resonance region of ^{182}W extended to 10 keV.

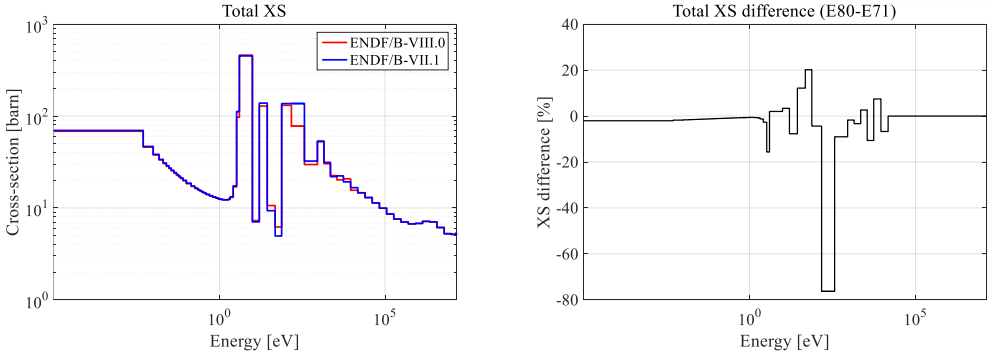

Figure 73. W-182 Total XS and XS difference with ENDF/B-VIII.0 and ENDF/B-VII.1 at 293.6K

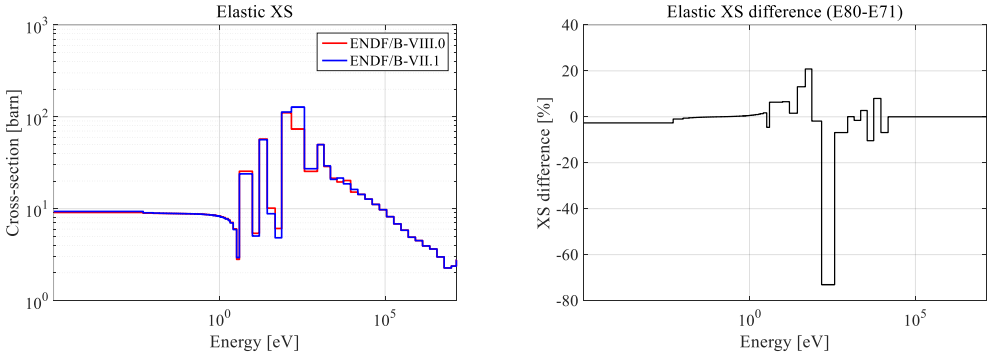

Figure 74. W-182 Elastic XS and XS difference with ENDF/B-VIII.0 and ENDF/B-VII.1 at 293.6K

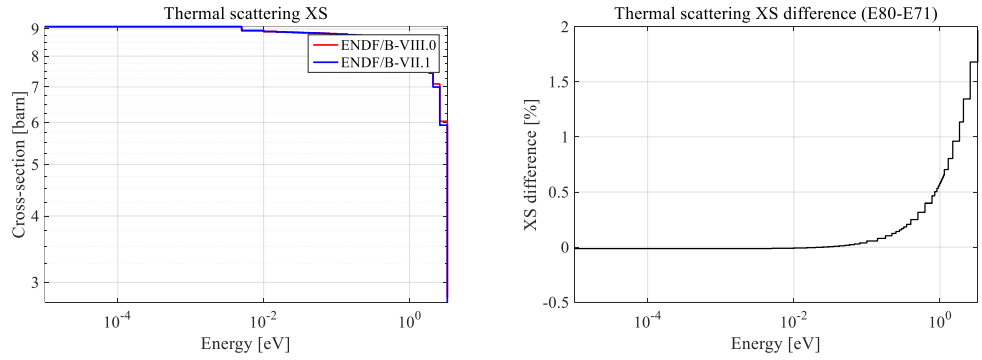

Figure 75. W-182 Thermal scattering XS and XS difference with ENDF/B-VIII.0 and ENDF/B-VII.1 at 293.6K

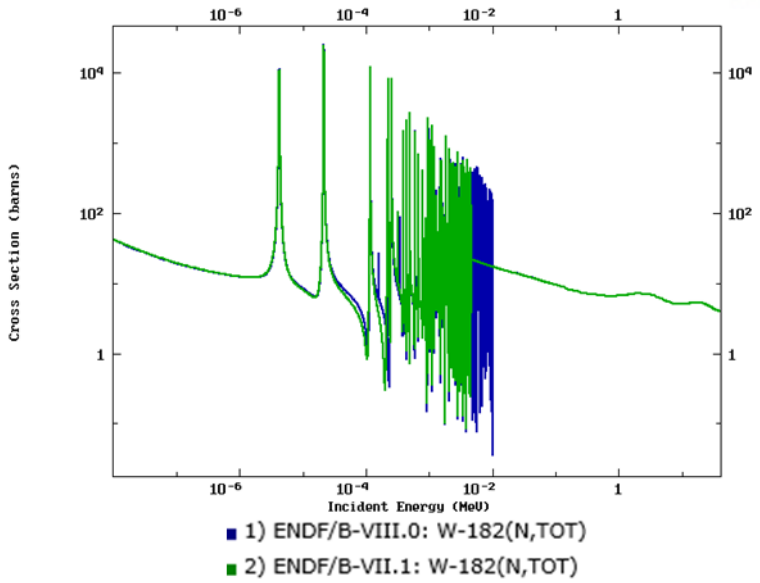

Figure 76. W-182 Total XS with ENDF/B-VIII.0 and ENDF/B-VII.1

6.17. 74-W-183 ENDF/B-VIII.0 & ENDF/B-VII.1 XS difference (293.6K)

In the ENDF/B-VIII.0 library evaluation, the resonance region of ^{183}W has been further expanded. In the ENDF/B-VII.1 library released, the resonance region of ^{183}W were extended to 760 eV, and now in the ENDF/B-VIII.0 library released, the resonance region of ^{183}W extended to 5 keV. Additionally, there is a significant discrepancy between the ENDF/B-VII.1 XS value and the ENDF/B-VIII.0 XS value at the thermal scattering XS of ^{183}W. The ENDF/B-VIII.0 XS of thermal scattering XS is significantly increased by ~140%. Also in the thermal region under 9.98 eV, Elastic XS of ^{183}W is increased by ~133%.

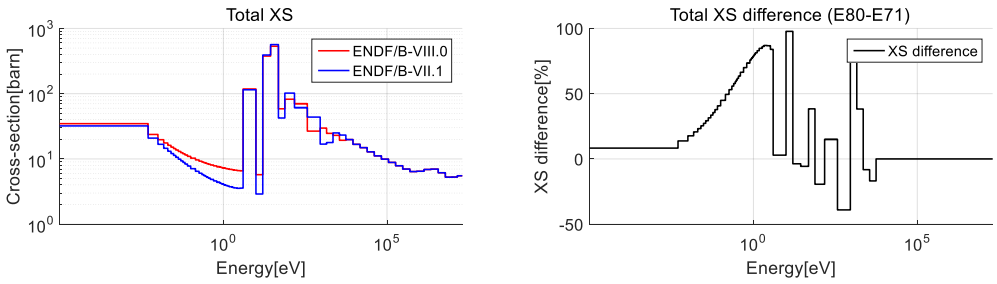

Figure 77. W-183 Total XS and XS difference with ENDF/B-VIII.0 and ENDF/B-VII.1 at 293.6K

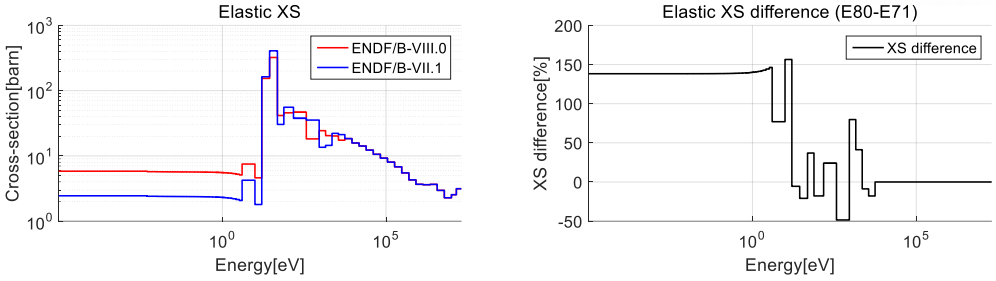

Figure 78. W-183 Elastic XS and XS difference with ENDF/B-VIII.0 and ENDF/B-VII.1 at 293.6K

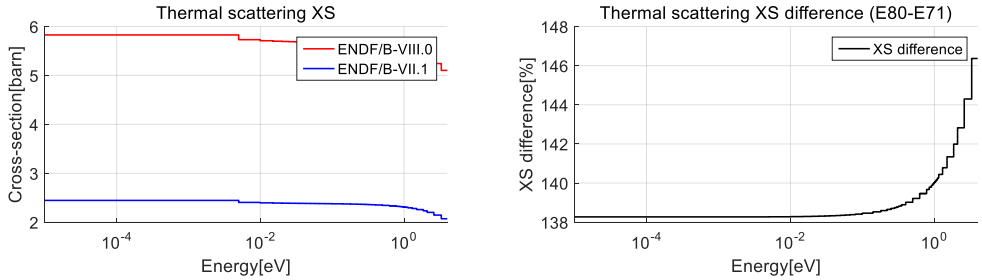

Figure 79. W-183 Thermal scattering XS and XS difference with ENDF/B-VIII.0 and ENDF/B-VII.1 at 293.6K

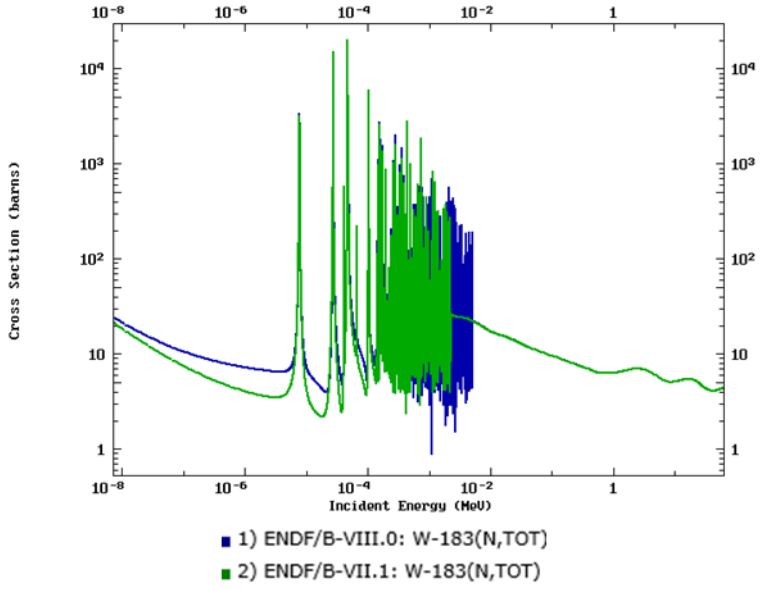

Figure 80. W-183 Total XS with ENDF/B-VIII.0 and ENDF/B-VII.1

6.18. 74-W-184 ENDF/B-VIII.0 & ENDF/B-VII.1 XS difference (293.6K)

In the ENDF/B-VIII.0 library evaluation, the resonance region of ^{184}W has been further expanded. In the ENDF/B-VII.1 library released, the resonance region of ^{184}W were extended to 4 keV, and now in the ENDF/B-VIII.0 library released, the resonance region of ^{184}W extended to 10 keV. In the resonance region between 48 eV to 9.1 keV, the elastic XS of ENDF/B-VIII.0 is changed from -30% to 10%.

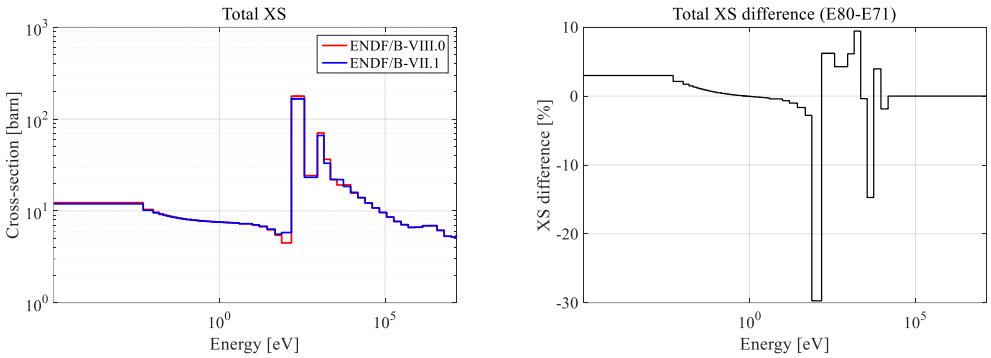

Figure 81. W-184 Total XS and XS difference with ENDF/B-VIII.0 and ENDF/B-VII.1 at 293.6K

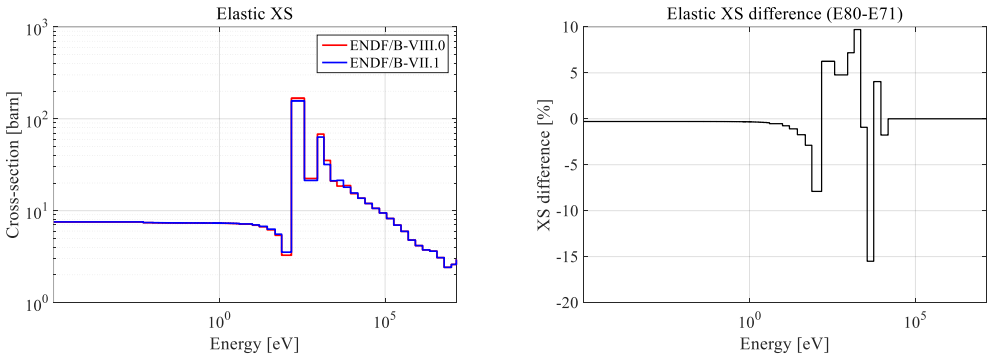

Figure 82. W-184 Elastic XS and XS difference with ENDF/B-VIII.0 and ENDF/B-VII.1 at 293.6K

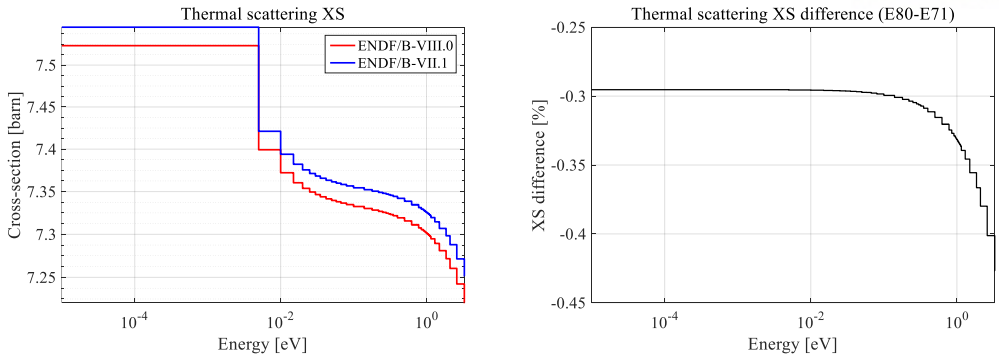

Figure 83. W-184 Thermal scattering XS and XS difference with ENDF/B-VIII.0 and ENDF/B-VII.1 at 293.6K

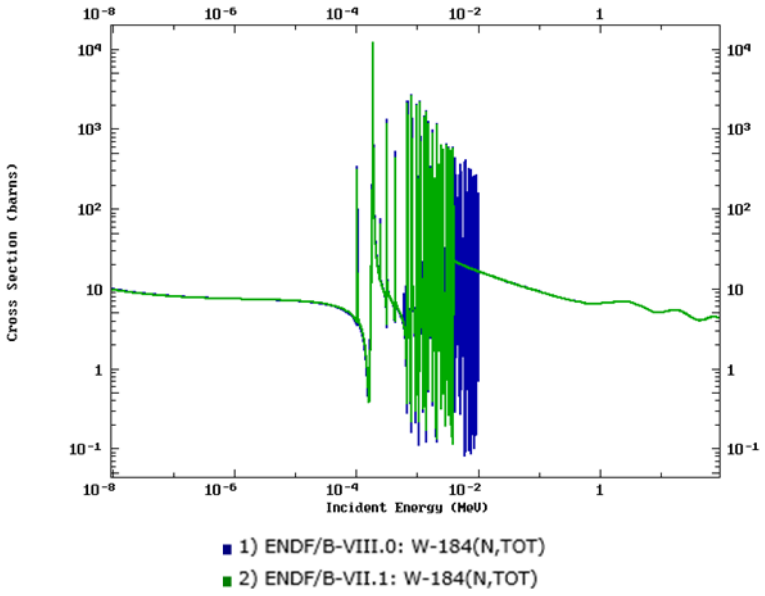

Figure 84. W-184 Total XS with ENDF/B-VIII.0 and ENDF/B-VII.1

6.19. 74-W-186 ENDF/B-VIII.0 & ENDF/B-VII.1 XS difference (293.6K)

In the ENDF/B-VII.1 library released, the resonance region of ^{186}W were extended to 8.5 keV, and now in the ENDF/B-VIII.0 library released, the resonance region of ^{186}W extended to 10 keV. In the resonance region between 48 eV to 9.1 keV, the elastic XS of ENDF/B-VIII.0 is changed from -15% to 30%.

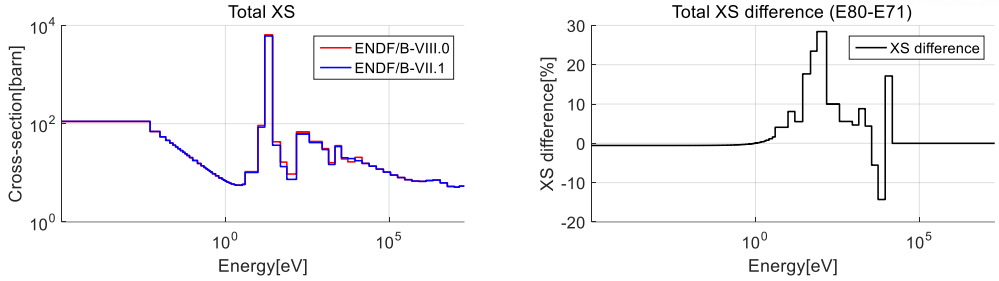

Figure 85. W-186 Total XS and XS difference with ENDF/B-VIII.0 and ENDF/B-VII.1 at 293.6K

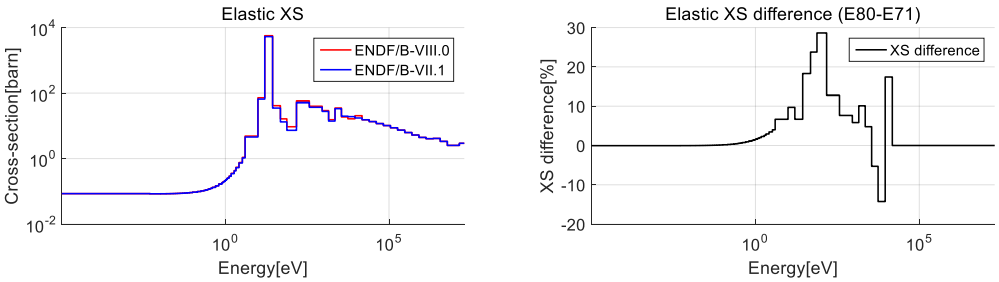

Figure 86. W-186 Elastic XS and XS difference with ENDF/B-VIII.0 and ENDF/B-VII.1 at 293.6K

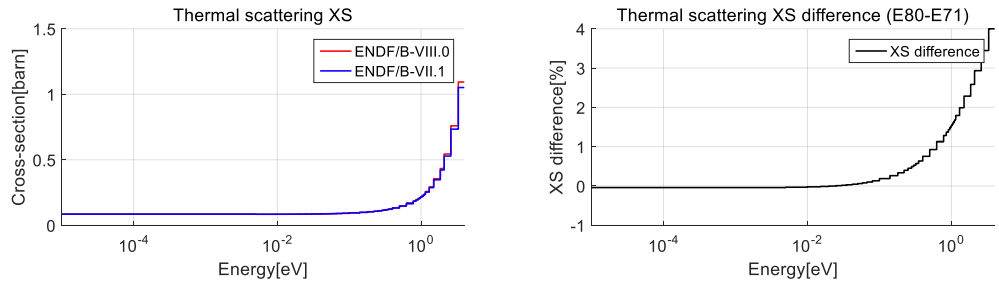

Figure 87. W-186 Thermal scattering XS and XS difference with ENDF/B-VIII.0 and ENDF/B-VII.1 at 293.6K

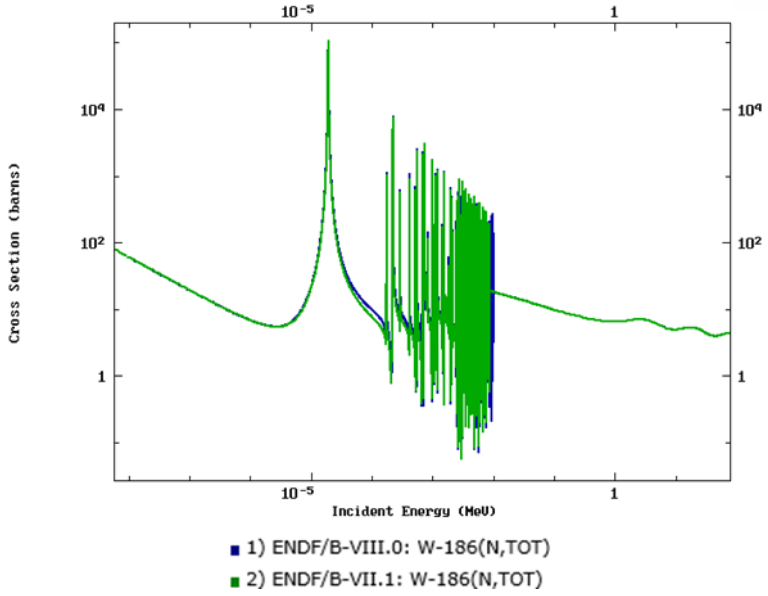

Figure 88. W-186 Total XS with ENDF/B-VIII.0 and ENDF/B-VII.1

VII. NCA BENCHMARK RESULTS

At the Toshiba NCA facility, 5 core experiments were performed about PWR condition at room temperature and at atmospheric pressure. NCA facility is a tank type light water moderated nuclear facility. There is two main region in the core. One is driver region that is filled by 2wt% enriched fuel rods. Another one is test region that is filled by various enriched fuel pin and experimental measured materials. Some of them included Tungsten gray control rods and some of them has polystyrene blocks with pin. Tungsten gray control rods is used in AP1000 PWR reactor, and to simulate the operating conditions (high pressure and high temperature) of light water reactor, polystyrene block containing boron carbide material is introduced to core.

As shown Table 2, Core 1,2 and 3 use tungsten gray rods, and Core 3 and 4 use borated polystyrene and Core 5 use polystyrene. Cores 1 and 5 are composed of 27×27 square pitches of length 1.52 cm. Cores 2, 3, and 4 are composed of 31×31 square pitches of the same size. All of the fuel pellets have a radius of 0.50 cm. The cladding, which is made of aluminum, has an outer radius of 0.59 cm and a thickness of 0.08 cm. The UO2 fuel density is 10.4 g/cm3 except for poisoned pellets. The density of fuel pellets with gadolinium is 10.1 g/cm3. The polystyrene density is 1.04g/cm3.

Core 1 configuration

Core 1 contains 25 tungsten gray rods and twelve 2wt% fuel rods with 5wt% of Gadolinium for a burnable absorber. It has various fuel enrichments ranging : 2wt% ~ 4.9wt%. The tungsten rods diameter is 0.5 and it use natural tungsten material. In the experiments, the axial length of tungsten rod is 50 cm (50% of the total rod length). The purpose of this experiment is the measurements of the reactivity and the fission rates.

Core 2 configuration

Core 2 has a simpler structure than other cores. It has only 2wt% enriched fuel rods and twelve tungsten gray rods. The tungsten rods diameter is 0.5 cm, In the experiments, the axial length of tungsten rods is 30 cm (Only covering the lower part of core). The purpose of this experiment

is to measure the tungsten reactivity worth and pin power distribution in the presence of the tungsten rod.

Core 3 configuration

Core 3 has two types of fuel rods; 2 wt% and 4.9 wt% fuel rods and total four tungsten gray rods. The tungsten rods diameter is 0.5 cm. In the experiments, the axial length of tungsten rods is 110 cm (Covering whole range of the critical water height). These pins on the test region are encircled by a polystyrene block containing 1000 ppm of boron. The polystyrene blocks radius is 0.6124 cm and total 4 stainless steel rods as a support for the polystyrene block sheet. It is representing hot full power condition.

Core 4 configuration

Core 4 has various fuel enrichments ranging from 2wt% to 4.9wt% and twelve 2wt% of a uranium enriched fuel rods with 5wt% of Gadolinium burnable absorber. It has 25 water holes with boric acid water. The boric acid water contain 1000 ppm of boron. Polystyrene blocks specification is same with Core 3. This core is designed to simulate the beginning of cycle (BOC) conditions of a PWR reactor.

Core 5 configuration

Core 5 also has various fuel enrichments ranging from 2wt% to 3.9wt%, but it is not containing 4.9wt% enriched fuel pin. It has 25 water holes with no boric acid water. These pins on the test region are encircled by a polystyrene bloc. The polystyrene contains no boron. The polystyrene blocks radius is 0.6124 cm and total 4 stainless steel rods as a support for the polystyrene block sheet. This core was designed to simulate the end of cycle (EOC) conditions of a PWR reactor.

Table 2. The five core configurations.

Core number	Tungsten	Polystyrene Block	Boron in Block	Gadolinium	Assembly
1	25 pins			12 pins	27 x 27
2	12 pins				31 x 31
3	4 pins	13 x 13 pins	O		31 x 31
4		21 x 21 pins	O	12 pins	31 x 31
5		21 x 21 pins			27 x 27

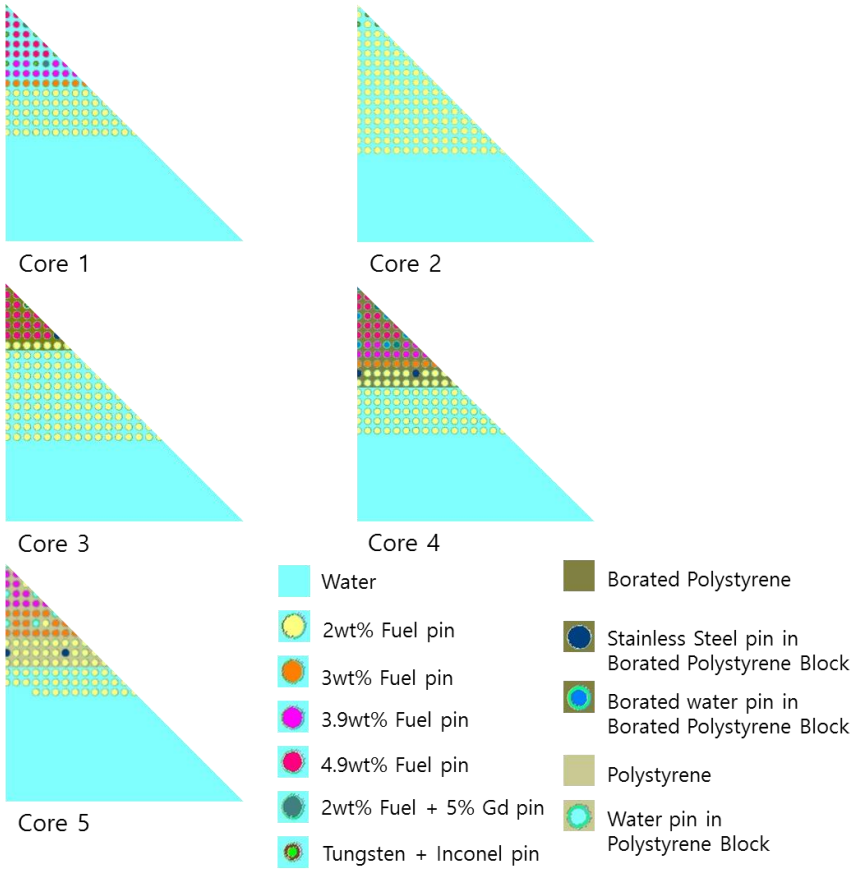

Figure 89. NCA Core configurations.

Table 3 and 4 show the comparison of the eigenvalue results of ENDF/B-VIII.0 between STREAM and MCS. As shown, Table 3 use ENDF/B-VIII.0 XS library and Table 4 use ENDF/B-VII.1 XS library. MCS and STREAM has small differences of k values within 84pcm with both of XS library. In MCS, 2-dimensional models were designed with 500,000 neutron histories in 500 active cycles. Statistical error is 5pcm for eigenvalues. Additionally for checking accuracy of MCS code, Monte Carlo codes, MCNP6 is used. In MCNP6, 2-dimensional models were designed with 600,000 neutron histories in 1,000 active cycles. Statistical error is 3pcm for eigenvalues. In case of ENDF/B-VIII.0, MCNP6 results is not

given, because MCNP6 XS system of ENDF/B-VIII.0 is not constructed.

Table 3. NCA Benchmark Multiplication factor comparison of ENDF/B-VIII.0

CORE Number	STREAM	MCS	Delta k (STREAM-MCS)
1	1.00350	1.00309(5)	41
2	1.02877	1.02861(5)	16
3	1.03816	1.03732(5)	84
4	0.97079	0.97046(5)	33
5	0.99845	0.99832(5)	13

Table 4. NCA Benchmark Multiplication factor comparison of ENDF/B-VII.1

CORE Number	MCNP6	STREAM	MCS	Delta k (STREAM-MCS)	Delta k (STREAM-MCNP6)	Delta k (MCS-MCNP6)
1	1.00396(3)	1.00455	1.00435(5)	20	59	39
2	1.02941(3)	1.02957	1.02966(5)	-9	16	25
3	1.03894(3)	1.03907	1.03834(5)	73	13	-60
4	0.97106(3)	0.97128	0.97118(5)	10	22	12
5	0.99963(3)	0.99970	0.99989(5)	-19	7	26

Table 5. NCA Benchmark Multiplication factor comparison of ENDF/B-VII.0

CORE Number	MCNP6	STREAM	MCS	Delta k (STREAM-MCS)	Delta k (STREAM-MCNP6)	Delta k (MCS-MCNP6)
1	1.00396(3)	1.00433	1.00390(5)	65	37	-28
2	1.02930(3)	1.02949	1.02956(5)	30	19	-11
3	1.03904(3)	1.03908	1.03847(5)	61	4	-57
4	0.97117(3)	0.97138	0.97125(5)	29	21	8
5	0.99975(3)	0.99976	0.99980(5)	-4	1	5

Table 6. NCA Benchmark Multiplication factor comparison between ENDF/B-VIII.0 and ENDF/B-VII.1

CORE Number	STREAM(E71)	STREAM(E80)	Delta k (E80-E71) (STREAM)	MCS(E71)	MCS(E80)	Delta k (E80-E71) (MCS)
1	1.00455	1.00350	-105	1.00435(5)	1.00309(5)	-126
2	1.02957	1.02877	-80	1.02966(5)	1.02861(5)	-105
3	1.03907	1.03816	-91	1.03834(5)	1.03732(5)	-102
4	0.97128	0.97079	-49	0.97118(5)	0.97046(5)	-72
5	0.99970	0.99845	-125	0.99989(5)	0.99832(5)	-157

Figure 90~94 is the pin power distribution comparison with STREAM results with each ENDF library versions and NCA benchmark measurement data

100(STREAM-Meas.)/STREAM ENDF/B-VIII.0 RMS 0.73648

0.000								
0.756	0.443							
0.584	0.647	**-0.956**						
0.000	0.210	0.909	0.000					
1.148	0.321	0.179	0.818	0.395				
0.986	0.449	0.299	0.597	1.183	0.000			
0.000	0.301	0.444	0.000	-0.852	0.319	-0.270		
-0.622	-0.474	-0.690	0.071	-0.578	-0.431	-0.669	-0.446	
0.674	1.130	0.782	0.917	1.212	0.919	1.033	1.016	**1.225**

100(STREAM-Meas.)/STREAM ENDF/B-VII.1 RMS 0.75057

0.000								
0.843	0.541							
0.600	0.605	**-1.060**						
0.000	0.231	0.866	0.000					
1.241	0.422	0.208	0.845	0.431				
1.080	0.549	0.404	0.555	1.002	0.000			
0.000	0.349	0.496	0.000	-0.952	0.171	-0.270		
-0.577	-0.424	-0.636	0.055	-0.729	-0.508	-0.669	-0.370	
0.675	1.208	0.786	0.926	1.225	0.937	0.978	0.965	1.175

100(STREAM-Meas.)/STREAM ENDF/B-VII.0 RMS 0.74453

0.000								
0.817	0.516							
0.573	0.581	**-1.063**						
0.000	0.205	0.842	0.000					
1.214	0.396	0.259	0.820	0.407				
1.054	0.524	0.379	0.531	0.980	0.000			
0.000	0.327	0.475	0.000	-0.879	0.153	-0.289		
-0.600	-0.446	-0.658	0.034	-0.672	-0.451	-0.613	-0.389	
0.732	1.190	0.844	0.908	1.208	0.920	1.037	1.025	**1.235**

Figure 90. NCA Core 1 Pin power distribution comparison with STREAM and Measurement data by ENDF/B-VIII.0, ENDF/B-VII.1 and ENDF/B-VII.0.

100(STREAM-Meas.)/STREAM	ENDF/B-VIII.0	RMS	1.01009			
-0.899						
0.015	0.000					
0.000	0.525	0.000				
1.444	1.938	0.061	-1.015			
0.715	-0.362	**-1.296**	-0.150	0.429		
-1.207	1.792	-0.767	1.125	0.569	0.743	
-0.700	-0.602	0.239	-0.225	0.464	1.093	**2.292**

100(STREAM-Meas.)/STREAM	ENDF/B-VII.1	RMS	1.05538			
-1.275						
-0.361	0.000					
0.000	0.300	0.000				
1.370	1.865	-0.012	-0.937			
0.717	-0.284	**-1.218**	-0.072	0.582		
-1.129	1.870	-0.614	1.278	0.722	0.897	
-0.547	-0.448	0.392	0.004	0.693	1.322	**2.521**

100(STREAM-Meas.)/STREAM	ENDF/B-VII.0	RMS	1.059			
-1.506						
-0.667	0.000					
0.000	0.069	0.000				
1.215	1.710	-0.091	-1.017			
0.638	-0.364	**-1.298**	-0.075	0.503		
-1.132	1.866	-0.693	1.275	0.719	0.893	
-0.550	-0.452	0.389	0.001	0.689	1.318	**2.518**

Figure 91. NCA Core 2 Pin power distribution comparison with STREAM and Measurement data by ENDF/B-VIII.0, ENDF/B-VII.1 and ENDF/B-VII.0.

100(STREAM-Meas.)/STREAM	ENDF/B-VIII.0	RMS	1.58443			
1.522						
0.970	1.932					
1.686	1.595	0.000				
1.328	1.487	1.629	1.657			
0.536	1.133	0.628	1.177	1.397		
0.340	1.489	0.541	1.429	**2.235**	0.000	
-0.583	**-3.844**	-2.572	-2.212	-0.771	-1.094	0.384

100(STREAM-Meas.)/STREAM	ENDF/B-VII.1	RMS	1.53225			
1.550						
0.928	1.887					
1.713	1.611	0.000				
1.358	1.444	1.647	1.615			
0.492	1.089	0.584	1.064	1.280		
0.336	1.485	0.538	1.362	**2.161**	0.000	
-0.375	**-3.739**	-2.356	-2.105	-0.669	-1.005	0.452

100(STREAM-Meas.)/STREAM	ENDF/B-VII.0	RMS	1.5226			
1.494						
0.941	1.900					
1.657	1.557	0.000				
1.372	1.458	1.593	1.629			
0.505	1.102	0.598	1.077	1.293		
0.350	1.499	0.552	1.375	**2.113**	0.000	
-0.361	**-3.725**	-2.342	-2.091	-0.655	-0.991	0.466

Figure 92. NCA Core 3 Pin power distribution comparison with STREAM and Measurement data by ENDF/B-VIII.0, ENDF/B-VII.1 and ENDF/B-VII.0.

100(STREAM-Meas.)/STREAM ENDF/B-VIII.0 RMS 1.70317

0.000								
1.712	3.516							
2.536	2.769	0.506						
0.000	1.524	1.171	0.000					
0.437	3.929	2.153	-0.250	1.760				
2.052	**4.397**	2.317	0.706	2.405	0.000			
0.000	-0.014	0.912	0.000	0.442	0.339	0.686		
-0.415	0.835	0.314	**-0.675**	0.544	0.206	0.349	1.209	
1.297	1.596	0.000	1.462	0.000	1.089	1.390	0.722	0.637

100(STREAM-Meas.)/STREAM ENDF/B-VII.1 RMS 1.72325

0.000								
1.953	3.621							
2.704	2.728	0.299						
0.000	1.697	1.279	0.000					
0.602	3.953	2.182	-0.153	1.714				
2.138	**4.419**	2.344	0.732	2.286	0.000			
0.000	0.117	0.970	0.000	0.241	0.274	0.622		
-0.367	0.816	0.300	**-0.686**	0.400	0.063	0.286	1.067	
1.321	1.621	0.000	1.494	0.000	1.054	1.359	0.615	0.607

Figure 93. NCA Core 4 Pin power distribution comparison with STREAM and Measurement data by ENDF/B-VIII.0 and ENDF/B-VII.1.

100(STREAM-Meas.)/STREAM ENDF/B-VIII.0 RMS 3.16649

0.000								
4.623	**5.922**							
4.624	5.031	2.937						
0.000	3.054	2.970	0.000					
3.846	2.898	3.855	1.312	1.954				
4.102	5.145	4.841	3.287	1.601	0.000			
0.000	4.562	3.390	0.000	0.309	1.678	1.804		
2.984	4.793	4.523	0.732	2.169	2.470	2.213	1.957	
1.328	0.964	0.000	1.404	0.000	-0.526	1.120	**-0.567**	0.039

100(STREAM-Meas.)/STREAM ENDF/B-VII.1 RMS 3.19503

0.000								
4.858	**5.941**							
4.784	5.129	3.139						
0.000	3.220	3.135	0.000					
3.937	2.853	3.891	1.329	1.905				
4.198	5.180	4.876	3.385	1.697	0.000			
0.000	4.586	3.416	0.000	0.357	1.725	1.730		
2.938	4.684	4.418	0.695	2.075	2.396	2.080	1.759	
1.321	0.880	0.000	1.327	0.000	-0.585	0.993	**-0.605**	-0.070

Figure 94. NCA Core 5 Pin power distribution comparison with STREAM and Measurement data by ENDF/B-VIII.0 and ENDF/B-VII.1.

VIII. ICSBEP BENCHMARK RESULTS

The International Criticality Safety Benchmark Evaluation Project (ICSBEP) became an official activity of the Organization for Economic Cooperation and Development - Nuclear Energy Agency (OECD-NEA) in 1995. It contains criticality safety benchmark specifications that have been derived from experiments performed at various nuclear critical facilities around the world. The evaluated criticality safety benchmark contain 567 evaluations with benchmark specifications for 4,874 critical, near critical or subcritical configurations, 31 criticality alarm placement / shielding configurations with multiple dose points for each, and 207 configurations that have been categorized as fundamental physics measurements that are relevant to criticality safety applications.

In the ICSBEP Benchmark, there are lots of critical experiment shape. However in this paper, only experiments that could be implemented as R-Z models were adopted for STREAM validation. It contains only cylindrical geometry except to spherical assembly. All benchmarks are subdivided into the main categories according to three criteria presented in Table 11. Benchmark systems and descriptions are shown in Table 12.

In Table 12, PU-MET-INTER-004 problem is also from ZPR-3 facility. So all ICSBEP Benchmark problem in this research is from ZPR program. ZPR is an acronym for Zero Power Reactor, referring to the four very similar fast-reactor critical experiment facilities at Argonne. This assembly provides a useful benchmark for testing criticality calculations for MOC codes. The ZPR-3 facility was a horizontal type, and formed a 31x31 square matrix. It can have a different matrix map on front and back. The simulation is based on the Stationary-Half Front Drawer Matrix Map, so the simulation results can be different with experimental effective results. Therefore, MCS input is matched equally on STREAM input.

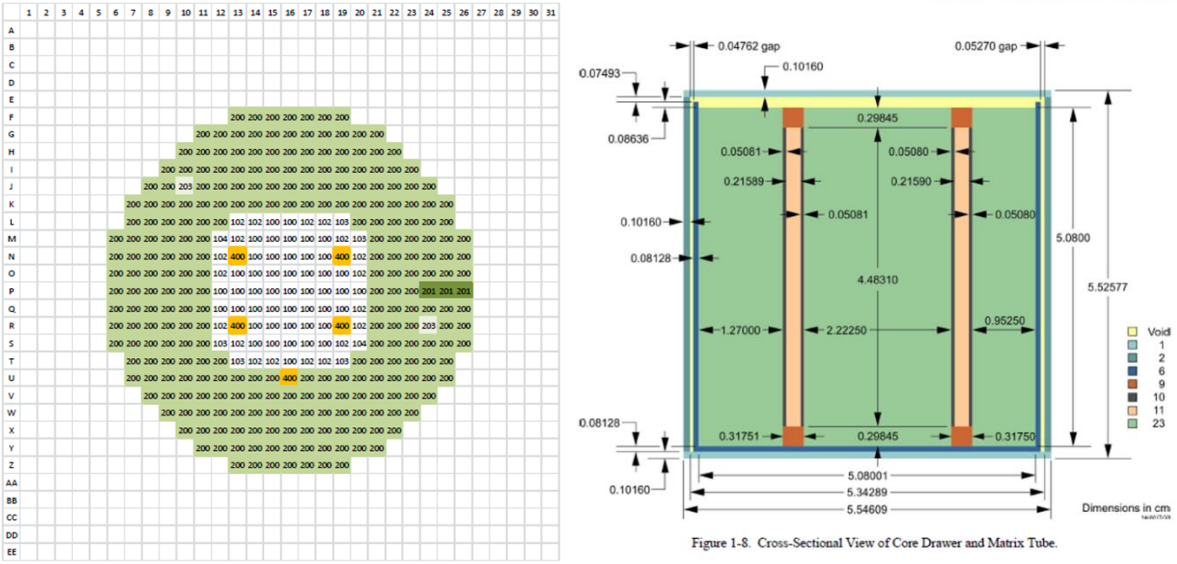

Figure 96. PU-MET-INTER-004; ZPR-3 Assembly 59 Stationary Front-Drawer Loading & Cross-sectional View of Core Drawer

Table 11. ICSBEP Benchmark abbreviations meaning

Abbreviation	Meaning
Fissile material	
HEU	High enriched uranium (U-235 > 60 wt%)
IEU	Intermediate or mixed enrichment uranium (60 wt% > 235U > 10 wt%)
PU	Plutonium
MIX	Mixed uranium and plutonium
Physical form of fissile material	
MET	Metal
SOL	Solution
COMP	Compound system, e.g., lattice in water
Spectrum	
FAST	Fast system (50% of fissions above 100 keV)
INTER	Intermediate -Energy system
THERM	Thermal system (50% of fissions below 0.625 eV)

Table 12. ICSBEP Benchmark systems and descriptions

ICSBEP System	Description
HEU-MET-INTER-001	The Uranium/Iron Benchmark Assembly: A 235U(93%)/Iron Cylinder Reflected by Stainless Steel
HEU-MET-FAST-055	ZPR-3 Assembly 23: A Cylindrical Assembly of U Metal (93% 235U) and Aluminum Reflected by Depleted-Uranium
HEU-MET-FAST-060	ZPR-9 Assembly 4: A Cylindrical Assembly of U Metal (93% 235U) and Tungsten with Aluminum Reflectors
PU-MET-INTER-002	ZPR-6 Assembly 10: A Cylindrical Plutonium/Carbon/Stainless Steel Assembly with Stainless Steel and Iron Reflectors
PU-MET-INTER-003	ZPR-3 Assembly 58: A Cylindrical Assembly of Plutonium Metal and Graphite with a Thick Depleted Uranium Reflector
PU-MET-INTER-004	ZPR-3 Assembly 59: A Cylindrical Assembly of Plutonium Metal and Graphite with a Thick Lead Reflector
IEU-MET-FAST-013	ZPR-9 Assembly 1: A Cylindrical Assembly of U Metal (93% 235U) and Depleted Uranium with Aluminum Reflectors
IEU-MET-FAST-016	ZPR-3 Assembly 11: A Cylindrical Assembly of Highly Enriched Uranium and Depleted Uranium with an Average 235U Enrichment of 12 Atom % and a Depleted Uranium Reflector
MIX-MET-INTER-003	ZPR-3 Assembly 54: A Cylindrical Assembly of Plutonium Metal, Depleted Uranium and Graphite with a Thick Iron Reflector
MIX-MET-INTER-004	ZPR-3 Assembly 53: A Cylindrical Assembly of Plutonium Metal, Depleted Uranium and Graphite with a Thick Depleted Uranium Reflector

As a results, in case of HEU-MET-INTER-001, U-235 is 93% enriched and Fe atoms contained 7.00690 x 10^-2 atoms/barn-cm in the core. Under the iron dominant condition, STREAM ENDF/B-VIII.0 results is 184pcm smaller than STREAM ENDF/B-VII.1 results. XS change of Fe atoms by ENDF/B-VIII.0 is significant, so it can be affected on the results. In case of HEU-MET-FAST-055 and HEU-MET-FAST-060, the difference is whether the tungsten is or is not. At ENDF/B-VIII.0, the multiplication factor difference between STREAM & MCS is within -73 on those two cases. It looks that the tungsten XS difference effect between ENDF/B-VIII.0 and ENDF/B-VII.1 is not too big to effect significantly on multiplication factor.

As shown as Table 15, in ICSBEP benchmark cases using metallic fuel, STREAM ENDF/B-VIII.0 library is well-matched with MCS ENDF/B-VIII.0 results. When the STREAM results of ENDF/B-VIII.0 are compared as a whole with the results of STREAM ENDF/B-VII.1, it can be considered to fit within a maximum of 264 pcm. In MCS, 2-dimensional models were designed with 500,000 neutron histories in 500 active cycles. Statistical error is 5pcm for eigenvalues.

Table 13. ICSBEP Benchmark multiplication factor comparison (STREAM)

	Reference keff	Reference std.	STREAM ENDF 8.0	STREAM ENDF 7.1	Δk(E80-Ref.)	Δk(E80-E71)
HEU-MET-INTER-001	1.00060	0.00110	0.99089	0.99273	-787	-184
HEU-MET-FAST-055	1.00120	0.00260	0.99765	0.99818	-355	-53
HEU-MET-FAST-060	1.00130	0.00110	1.01011	1.01023	881	-12
PU-MET-INTER-002	1.00160	0.00130	0.98587	0.98688	-1573	-101
PU-MET-INTER-003	1.00020	0.00120	0.98983	0.98846	-1037	137
PU-MET-INTER-004	1.00080	0.00180	0.97720	0.97583	-2360	137
IEU-MET-FAST-013	1.00185	0.00100	1.01597	1.01787	1412	-190
IEU-MET-FAST-016	1.00130	0.00120	0.99664	0.99924	-466	-260
MIX-MET-INTER-003	1.00180	0.00110	0.97765	0.97586	-2415	179
MIX-MET-INTER-004	1.00180	0.00090	0.98490	0.98226	-1690	264

Table 14. ICSBEP Benchmark multiplication factor comparison (MCS) (std. 5 pcm)

	Reference keff	Reference std.	MCS ENDF 8.0	MCS ENDF 7.1	Δk(E80-Ref.)	Δk(E80-E71)
HEU-MET-INTER-001	1.00060	0.00110	0.99124	0.99295	-765	-171
HEU-MET-FAST-055	1.00120	0.00260	0.99834	0.99862	-286	-28
HEU-MET-FAST-060	1.00130	0.00110	1.01084	1.01041	2354	43
PU-MET-INTER-002	1.00160	0.00130	0.98585	0.98725	-1575	-140
PU-MET-INTER-003	1.00020	0.00120	0.98948	0.98854	-1072	94
PU-MET-INTER-004	1.00080	0.00180	0.97754	0.97581	-2326	173
IEU-MET-FAST-013	1.00185	0.00100	1.01671	1.01843	1486	-172
IEU-MET-FAST-016	1.00130	0.00120	0.99603	0.99866	-527	-263
MIX-MET-INTER-003	1.00180	0.00110	0.97749	0.97579	-2431	170
MIX-MET-INTER-004	1.00180	0.00090	0.98551	0.98260	-1629	291

Table 15. ICSBEP Benchmark multiplication factor comparison between STREAM & MCS (ENDF/B-VIII.0)

	STREAM ENDF 8.0	MCS ENDF 8.0	Δk(STREAM-MCS)(E80)
HEU-MET-INTER-001	0.99089	0.99124	-35
HEU-MET-FAST-055	0.99765	0.99834	-69
HEU-MET-FAST-060	1.02411	1.02484	-73
PU-MET-INTER-002	0.98587	0.98585	2
PU-MET-INTER-003	0.98983	0.98948	35
PU-MET-INTER-004	0.97720	0.97754	-34
IEU-MET-FAST-013	1.01597	1.01671	-74
IEU-MET-FAST-016	0.99664	0.99603	61
MIX-MET-INTER-003	0.97765	0.97749	16
MIX-MET-INTER-004	0.98490	0.98551	-61

XI. VERA BENCHMARK RESULTS

VERA Benchmark provide a reactor core problem models and data from the initial core loading of Watts Bar Nuclear 1, a Westinghouse-designed 17x17 Pressurized Water Reactor(PWR). Provided are the detailed specifications for the VERA Benchmark Problems 1 through 10. These problems provide the isotopes atom density of each materials, geometry structure and a reference solution from Monte Carlo neutron transport solution. In order to validate the ENDF/B-VIII.0, Problem 2A~2P have selected. Table 7 is the description of the problems and Figure 95 is the Lattice Layout of Problem 2A~2P. For this problem, KENO-VI can provide an approximate eigenvalue solution within a small range of uncertainty.

Fuel enrichment is the maximum of the three regions: 3.1% Fuel (Problem 2A~2J & 2L~2N), 3.6% Fuel (Problem 2K), 5% Gd2O3 & 95% UO2 1.8% Fuel (Problem 2O, 2P). Nominal fuel density is 10.257g/cc. The problem geometry is modeled in octant symmetry at STREAM. Reflective boundary conditions are applied on all sides. For Problem 2K, the low enriched rods are the same enrichment 3.1% as other problem. Problem 2E~2P has 600K fuel temperature, and Problem 2B~2P has 600K moderator temperature.

Table 7. The description of VERA Benchmark Problems

Problem Name	Description
VERA_2A	17x17 FA with no poison and 565K fuel
VERA_2B	17x17 FA with no poison and 600K fuel
VERA_2C	17x17 FA with no poison and 900K fuel
VERA_2D	17x17 FA with no poison and 1200K fuel
VERA_2E	17x17 FA with 12 Pyrex rods
VERA_2F	17x17 FA with 24 Pyrex rods
VERA_2G	17x17 FA with 24 AIC rods
VERA_2H	17x17 FA with 24 B4C rods
VERA_2I	17x17 FA with thimble
VERA_2J	17x17 FA with thimble and 24 Pyrex rods
VERA_2K	17x17 FA with zoned fuel and 24 Pyrex rods
VERA_2L	17x17 FA with 80 IFBA rods
VERA_2M	17x17 FA with 128 IFBA rods
VERA_2N	17x17 FA with 104 IFBA rods and 20 WABA
VERA_2O	17x17 FA with 12 Gadolinia
VERA_2P	17x17 FA with 24 Gadolinia

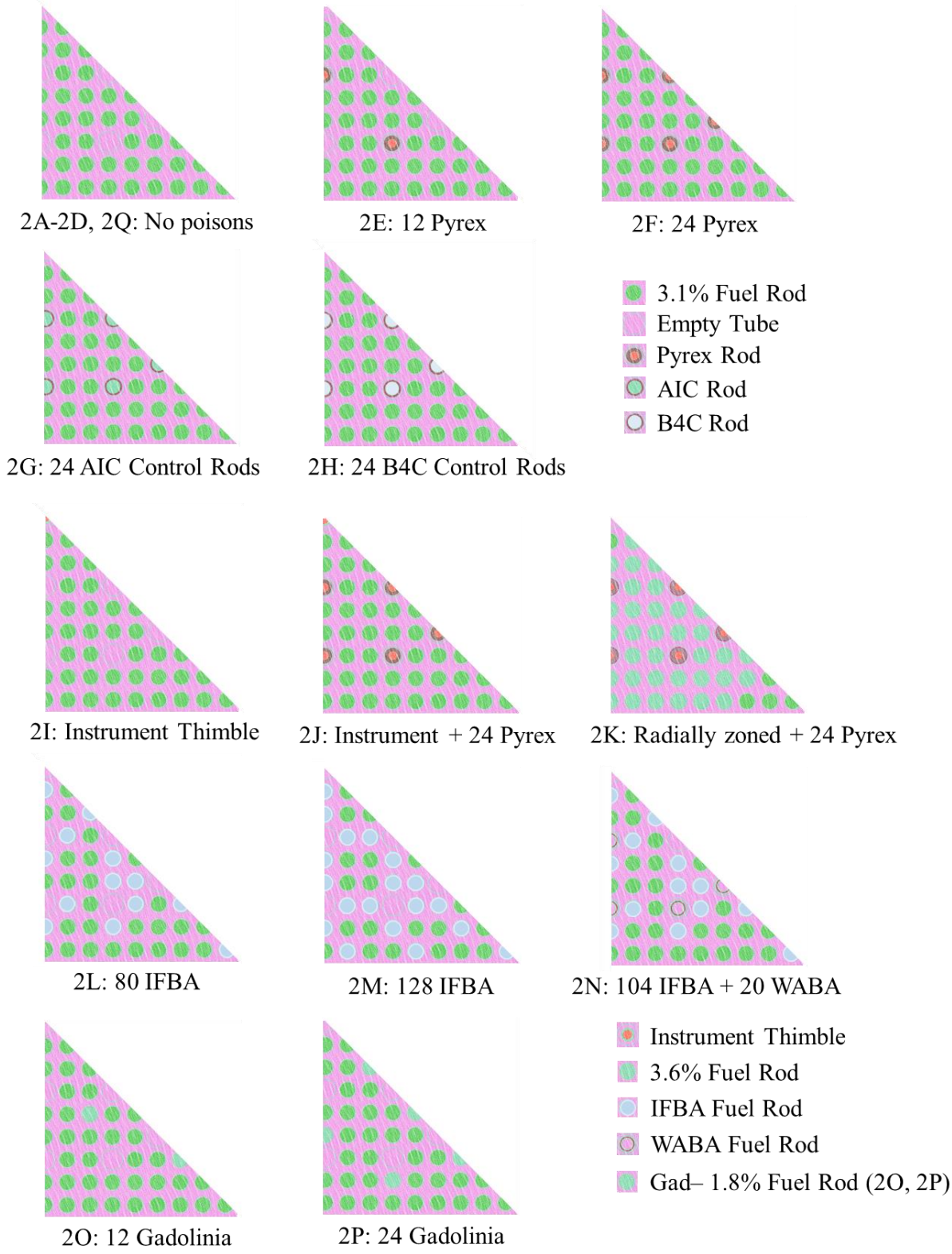

Figure 95. VERA Benchmark Problem 2A~2P Octant Symmetry Lattice Layout in STREAM

For the validation of STREAM ENDF/B-VIII.0 XS library, STREAM ENDF/B-VIII.0 results and STREAM ENDF/B-VII.1 results are compared. In Table 8, multiplication factor difference between STREAM ENDF/B-VIII.0 results and Reference value of most of cases is within 179pcm except to Problem 2G and Problem 2H. Moreover, except to Problem 2G and Problem 2H, the ENDF/B-VIII.0 results shows a tendency to match up the reference better than the ENDF/B-VII.1 results. In case of Problem 2G & 2H, they are containing 24 control rods; each are AIC Rod and B4C Rod. This tendency has also been seen in the Monte Carlo code, MCS results in Table 9. As shown as Table 10, STREAM ENDF/B-VIII.0 XS library results is up to -40pcm with comparing MCS results. In MCS, 2-dimensional models were designed with 500,000 neutron histories in 500 active cycles. Statistical error is 5pcm for eigenvalues.

Table 8. VERA benchmark multiplication factor comparison (STREAM)

	Reference keff	Reference std.	STREAM ENDF 8.0	STREAM ENDF 7.1	Delta k(E80-Ref.)	Delta k(E80-E71)
VERA_2A	1.182175	0.000017	1.18166	1.18075	-52	91
VERA_2B	1.183360	0.000024	1.18285	1.18203	-51	82
VERA_2C	1.173751	0.000023	1.17341	1.17251	-34	90
VERA_2D	1.165591	0.000023	1.16556	1.16461	-3	95
VERA_2E	1.069627	0.000024	1.07060	1.06886	97	174
VERA_2F	0.976018	0.000026	0.97773	0.97552	171	221
VERA_2G	0.847695	0.000025	0.85323	0.85082	554	241
VERA_2H	0.788221	0.000025	0.79265	0.79070	443	195
VERA_2I	1.179916	0.000024	1.17959	1.17856	-33	103
VERA_2J	0.975193	0.000025	0.97698	0.97478	179	220
VERA_2K	1.020063	0.000025	1.02135	1.01966	129	169
VERA_2L	1.018915	0.000024	1.01852	1.01589	-39	263
VERA_2M	0.938796	0.000025	0.93885	0.93557	5	328
VERA_2N	0.869615	0.000025	0.87073	0.86768	111	305
VERA_2O	1.047729	0.000024	1.04842	1.04634	69	208
VERA_2P	0.927410	0.000024	0.92867	0.92582	126	285

Table 9. VERA benchmark multiplication factor comparison (MCS) (std. 5 pcm)

	Reference keff	Reference std.	MCS ENDF 8.0	MCS ENDF 7.1	Delta k(E80-Ref.)	Delta k(E80-E71)
VERA_2A	1.182175	0.000017	1.18180	1.18086	-38	94
VERA_2B	1.183360	0.000024	1.18304	1.18213	-32	91
VERA_2C	1.173751	0.000023	1.17331	1.17233	-44	98
VERA_2D	1.165591	0.000023	1.16571	1.16480	12	91
VERA_2E	1.069627	0.000024	1.07028	1.06838	65	190
VERA_2F	0.976018	0.000026	0.97785	0.97572	183	213
VERA_2G	0.847695	0.000025	0.85290	0.85065	521	225
VERA_2H	0.788221	0.000025	0.79296	0.79082	474	214
VERA_2I	1.179916	0.000024	1.17968	1.17856	-24	112
VERA_2J	0.975193	0.000025	0.97679	0.97470	160	209
VERA_2K	1.020063	0.000025	1.02105	1.01929	99	176
VERA_2L	1.018915	0.000024	1.01892	1.01646	1	246
VERA_2M	0.938796	0.000025	0.93877	0.93555	-3	322
VERA_2N	0.869615	0.000025	0.87077	0.86763	116	314
VERA_2O	1.047729	0.000024	1.04867	1.04686	94	181
VERA_2P	0.927410	0.000024	0.92862	0.92578	121	284

Table 10. VERA benchmark multiplication factor comparison between STREAM & MCS (ENDF/B-VIII.0)

	STREAM ENDF 8.0	MCS ENDF 8.0	Delta k(STREAM-MCS)(E80)
VERA_2A	1.18166	1.18180	-14
VERA_2B	1.18285	1.18304	-19
VERA_2C	1.17341	1.17331	10
VERA_2D	1.16556	1.16571	-15
VERA_2E	1.07060	1.07028	32
VERA_2F	0.97773	0.97785	-12
VERA_2G	0.85323	0.85290	33
VERA_2H	0.79265	0.79296	-31
VERA_2I	1.17959	1.17968	-9
VERA_2J	0.97698	0.97679	19
VERA_2K	1.02135	1.02105	30
VERA_2L	1.01852	1.01892	-40
VERA_2M	0.93885	0.93877	8
VERA_2N	0.87073	0.87077	-4
VERA_2O	1.04842	1.04867	-25
VERA_2P	0.92867	0.92862	5

X. CONCLUSIONS

In this paper, the verification and validation of ENDF/B-VIII.0 XS data uses STREAM code and MCS code. ENDF/B-VIII.0 XS data compare with ENDF/B-VII.1 XS data. For making STREAM XS library for ENDF/B-VIII.0, The existing STREAM multi-group nuclear cross-section library generation system was divided into two stages; NJOY and NTOS, and the generation system was systematized by designating the file types required for each stage. Using the systematic STREAM XS library generation system, the 72G multi-group XS library for STREAM was generated based on the new ENDF/B-VIII.0 nuclear data library released in 2018. The produced STREAM XS library was also used to identify nuclear cross-section differences between ENDF/B-VIII.0 and ENDF/B-VII.1. Additionally, Using NJOY code, point-wise ACE XS file was generated ACE for MCS based on ENDF/B-VIII.0

Using this multi-group nuclear cross-section library, a total of three benchmark problems were simulated to verify the accuracy of the ENDF/B-VIII.0 XS library within the STREAM code. STREAM result of each benchmark was compared with reference data and the Monte Carlo code, MCS results, to assess the accuracy of the generated library. When the STREAM results produced by ENDF/B-VIII.0 were compared with Monte Carlo code results for each benchmark, and the difference in NCA Benchmark was found to be up to -157pcm, and in VERA Benchmark to 40pcm and in ICSBE Benchmark to -74pcm.

A normalized PWR neutron flux model was used on the NJOY multi-group XS production in GROUPR module, so it was expected to lead to slightly more errors in non-PWR models. When comparing ICSBEP results, it was found that on average, the error was twice as large as that of the model using fast energy region compared to the model using the intermediate energy region. In addition, the results of ENDF/B-VIII.0 were found to be closer to the reference and more accurate than those of ENDF/B-VII.1, except for a few exceptions, when compared with the value of the ICSBEP Benchmark reference. In case of fast reactor simulation, although the error of 72G ENDF/B-VIII.0 STREAM library on fast reactor problem is small enough, whether it can be applied to the fast reactor will require more simulation.

In this way, the accuracy of ENDF/B-VIII.0 XS in STREAM code was verified through the reproduction of nuclear data, analysis and verification of nuclear data. The ENDF/B-VIII.0 nuclear XS library generation system built in this paper will play a big role in generating and verifying the independent STREAM library when the future version of ENDF is released.

ACKNOWLEDGMENTS

REFERENCES

[1] Mohamed O, et al. “Analysis of tungsten gray rods critical experiments using PARAGON with ultra-fine energy mesh methodology.” *PHYSOR 2014*, Kyoto, Japan & September 25-October 3 (2014)

[2] Joshua H. and Rodolfo F. “CASMO5 Analysis of NCA tungsten critical experiments.” *ANFM 2015*, Hilton Head, SC&March 29-April 1 (2015)